The School of Mathematics

THE UNIVERSITY
of EDINBURGH

Robust Optimisation Monte Carlo for Likelihood-Free Inference

by

Vasileios Gkolemis

Dissertation Presented for the Degree of
MSc in Operational Research with Data Science

August 2020

Supervised by
Dr. Michael Gutmann

n

Abstract

Acknowledgments

Own Work Declaration

Here comes your own work declaration

Contents

List of Tables

List of Figures

1 Introduction

This dissertation is mainly focused on the implementation of the Robust Optimisation Monte Carlo (ROMC) method as it was proposed by (Ikonomov and Gutmann 2019) at the python package ELFI (Engine For Likelihood-Free Inference) (Lintusaari et al. 2018). The ROMC method describes a novel likelihood-free inference approach for simulator-based models.

1.1 Motivation

Explanation of simulation-based models

A simulator-based model is a parameterised stochastic data generating mechanism (Gutmann and Corander 2016). The key characteristic of these models is that although we can sample (simulate) data points, we cannot evaluate the likelihood for a specific set of observations $\mathbf{y_0}$. Formally, a simulator-based model is described as a parameterised family of probability density functions $\{p_{\mathbf{y}|\boldsymbol{\theta}}(\mathbf{y})\}_{\boldsymbol{\theta}}$, whose closed-form is either unknown or intractable to evaluate. Whereas evaluating $p_{\mathbf{y}|\boldsymbol{\theta}}(\mathbf{y})$ is intractable, sampling is feasible. Practically, a simulator can be understood as a black-box machine M_r[1] that given a set of parameters $\boldsymbol{\theta}$, produces samples $\mathbf{y}$ in a stochastic manner i.e. $M_r(\boldsymbol{\theta}) \rightarrow \mathbf{y}$.

Simulator-based models are particularly captivating due to the modelling freedom they provide; any physical process that can be conceptualised as a computer program of finite (deterministic or stochastic) steps can be modelled as a simulator-based model with any more mathematical compromise. This includes any amount of hidden (unobserved) internal variables or logic-based decisions. As always, this degree of freedom comes at a cost; performing the inference is particularly demanding from both the computational and the mathematical perspective. Unfortunately, the algorithms deployed so far, permit the inference only at low-dimensionality parametric spaces, i.e. $\boldsymbol{\theta} \in \mathbb{R}^D$ where D is small.

Example

For illustrating the importance of simulator-based models, let us use the tuberculosis disease spread example as described in (Tanaka et al. 2006). An overview of the disease spread model is presented at figure 1. At each stage one of the following *unobserved* events may happen; (a) the transmission of a specific haplotype to a new host (b) the mutation of an existent haplotype (c) the exclusion of an infectious host (recovers/dies) from the population. The random process, which stops when m infectious hosts are reached[2], can be parameterised (a) by the transmission rate α (b) the mutation rate τ and (c) the exclusion rate δ, creating a $3D$-parametric space $\boldsymbol{\theta} = (\alpha, \tau, \delta)$. The outcome of the process is a variable-size tuple $\mathbf{y}_{\boldsymbol{\theta}}$, containing the population contaminated by each different haplotype, as described in figure 1. Lets say that the disease has been spread in a real population and when m hosts where contaminated simultaneously, the vector with the infectious populations has been measured to be $\mathbf{y_0}$. We would like to discover the parameters $\boldsymbol{\theta} = (\alpha, \tau, \delta)$ that describe the spreading process and lead to the specific outcome $\mathbf{y_0}$. Computing $p(\mathbf{y} = \mathbf{y_0}|\boldsymbol{\theta})$ requires tracking all tree-paths that generate the specific tuple along with their probabilities and summing over them. Computing this probability by enumerating each possible tree-path that may lead to the specific outcome becomes intractable when m grows larger, as in real-case scenarios. This can be easily observed in the tree presented at figure 1. On the other hand, modelling the data-generation process as a computer program is simple and computationally efficient, hence using a simulator-based Model is a perfect fit.

Goal of Simulation-Based Models

As in most Machine Learning (ML) concepts, the fundamental goal is the derivation of one(many) parameter configuration(s) $\boldsymbol{\theta}^*$ that *describe* well the data i.e. generate samples $M_r(\boldsymbol{\theta}^*)$ that are as close as possible to the observed data $\mathbf{y_0}$. In our case, following the approach of Bayesian Machine

[1] The subscript r in M_r indicates the *random* simulator. In the next chapters we will introduce M_d witch stands for the *deterministic* simulator.

[2] We suppose that the unaffected population is infinite, so a new host can always be added until we reach m simultaneous hosts.

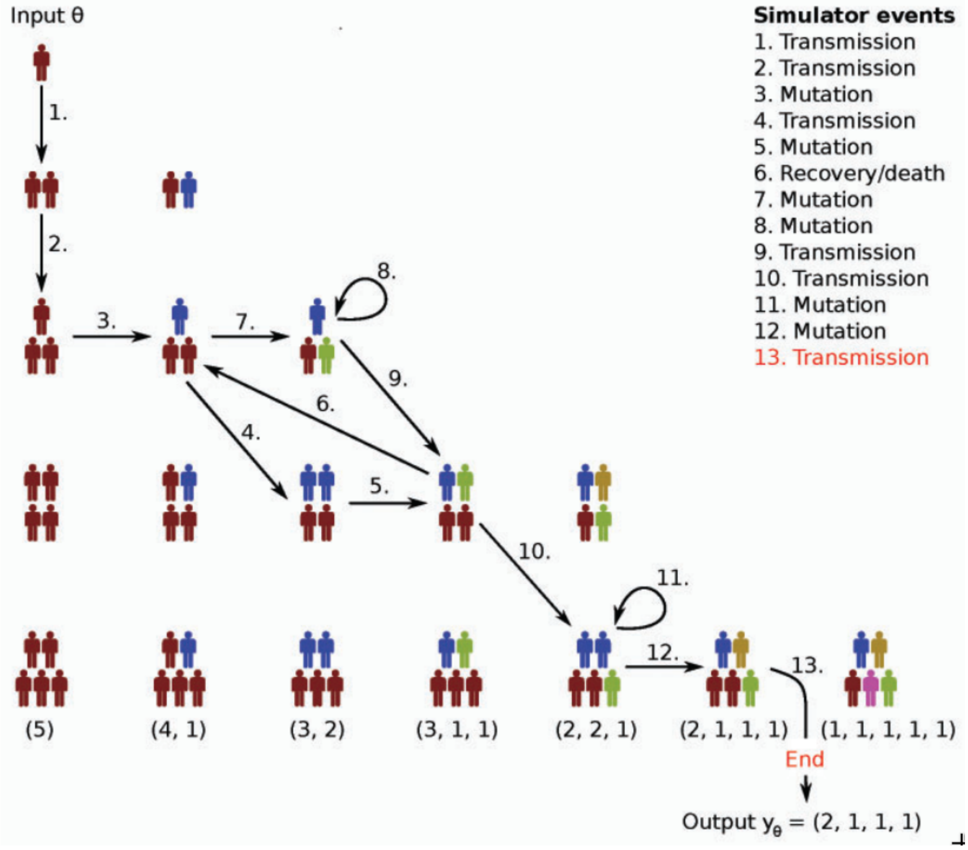

Figure 1: Depiction of a spread outcome of the tuberculosis spreading process. The image has been taken from (Lintusaari et al. 2017)

Learning, we treat the parameters of interest $\boldsymbol{\theta}$ as random variables and we try to *infer* a posterior distribution $p(\boldsymbol{\theta}|\mathbf{y_0})$ on them.

Robust Optimisation Monte Carlo (ROMC) method

The ROMC method (Ikonomov and Gutmann 2019) is very a recent Likelihood-Free approach; its fundamental idea is the transformation of the stochastic data generation process $M_r(\boldsymbol{\theta})$ to a deterministic mapping $g_i(\boldsymbol{\theta})$, by sampling the variables that produce the randomness $\mathbf{v}_i \sim p(\mathbf{V})$. Formally, in every stochastic process the randomness is influenced by a vector of random variables $\mathbf{V}$, whose state is unknown before the execution of the simulation; sampling the state makes the procedure deterministic, namely $g_i(\boldsymbol{\theta}) = M_d(\boldsymbol{\theta}, \mathbf{V} = \mathbf{v}_i)$. This approach initially introduced at (Meeds and Welling 2015) with the title *Optimisation Monte Carlo (OMC)*. The ROMC extended this approach by resolving a fundamental failure-mode of OMC. The ROMC describes a methodology for approximating the posterior through a series of algorithmic steps, without explicitly enforcing which algorithms must be utilised for each step[3]; in this sense, it can be thought as a meta-algorithm.

Implementation

The most important contribution of this work is the implementation of the ROMC method in the Python package Engine for Likelihood-Free Inference (ELFI) (Lintusaari et al. 2018). Since the method by published quite recently, if has not been implemented until now in any ML software. This work attempts to provide to the research community a tested and robust implementation for further experimentation and possible extensions.

[3] The implementation chooses a specific algorithm for each task, but this choice has just a demonstrative value; any appropriate algorithm can be used instead.

1.2 Outline of Thesis

The remainder of the dissertation is organised as follows. In Chapter 2, we establish the mathematical formulation; specifically, we initially describe the simulator-based models and provide some fundamental algorithms that have been proposed for performing inference in these set-ups. Afterwards, we provide the mathematical description of the ROMC approach (Ikonomov and Gutmann 2019). Finally, we depict the mathematical description into an algorithmic view. In Chapter 3, we illustrate the implementation part; we initially provide some information regarding the Python package Engine for Likelihood-Free Inference (ELFI) (Lintusaari et al. 2018) and subsequently, we present the implementation details of ROMC in this package. In general, the logical connectivity of the dissertation unit Chapter 3 follows the scheme; Mathematical modelling → Algorithm → Software.

In Chapter 4, we demonstrate the functionalities of the ROMC implementation at some real-world examples; this chapter desires to demonstrate the success of the ROMC method and our implementation's at Likelihood-Free tasks. Finally, in Chapter 5, we conclude with some thoughts on the work we have done and some future research ideas.

1.3 Notation

In this section, we provide an overview of the symbols utilised in the rest of the document. At this level, the quantities are introduced quite informally; most of them will be defined formally in the next chapters. We try to keep the notation as consistent as possible throughout the document. The symbol $\mathbb{R}^N$, when used, describes that a variable belongs to the $N-\textit{dimensional}$ euclidean space; N does not represent a specific number.

Random Generator

- $M_r(\boldsymbol{\theta}) : \mathbb{R}^D \rightarrow \mathbb{R}$: The black-box data simulator

Parameters/Random Variables/Symbols

- $D \in \mathbb{N}$, the dimensionality of the parameter-space
- $\boldsymbol{\Theta} \in \mathbb{R}^D$, random variable representing the parameters of interest
- $\mathbf{y_0} \in \mathbb{R}^N$, the vector with the observations
- $\epsilon \in R$, the threshold setting the limit on the region around $\mathbf{y_0}$
- $\mathbf{V} \in \mathbb{R}^N$, random variable representing the randomness of the generator. It is also called nuisance variable, because we are not interested in inferring a posterior distribution on it.
- $\mathbf{v}_i \sim \mathbf{V}$, a specific sample drawn from $\mathbf{V}$
- $\mathbf{Y}_{\boldsymbol{\theta}}$, random variable describing the simulator $M_r(\boldsymbol{\theta})$.
- $\mathbf{y}_i \sim \mathbf{Y}_\theta$, a sample drawn from $\mathbf{Y}_\theta$. It can be obtained by executing the simulator $\mathbf{y}_i \sim M_r(\boldsymbol{\theta})$

Sets

- $B_{d,\epsilon}(\mathbf{y_0})$, the set of $\mathbf{y}$ points close to the observations, i.e. $\mathbf{y} := \{\mathbf{y} : d(\mathbf{y}, \mathbf{y_0}) \leq \epsilon\}$
- $B^i_{d,\epsilon}$, the set of points defined around $\mathbf{y}_i$ i.e. $B^i_{d,\epsilon} = B_{d,\epsilon}(\mathbf{y}_i)$
- S_i, the set of $\boldsymbol{\theta}$ parameters that generate data close to the observations using the i-th deterministic generator, i.e. $\{\boldsymbol{\theta} : M_d(\boldsymbol{\theta}, \mathbf{v}_i) \in B_{d,\epsilon}(\mathbf{y_0})\}$

Generic Functions

- $p(\cdot)$, any valid pdf
- $p(\cdot|\cdot)$, any valid conditional distribution
- $p(\boldsymbol{\theta})$, the prior distribution on the parameters
- $p(\mathbf{v})$, the prior distribution on the nuisance variables
- $p(\boldsymbol{\theta}|\mathbf{y_0})$, the posterior distribution
- $p_{d,\epsilon}(\boldsymbol{\theta}|\mathbf{y_0})$, the approximate posterior distribution
- $d(\mathbf{x}, \mathbf{y}) : \mathbb{R}^{2N} \rightarrow \mathbb{R}$: any valid distance, the L_2 norm: $||\mathbf{x} - \mathbf{y}||_2$

Functions (Mappings)

- $M_d(\boldsymbol{\theta}, \mathbf{v}) : \mathbb{R}^D \rightarrow \mathbb{R}$, the deterministic generator; all stochastic variables that are part of the data generation process are represented by the parameter $\mathbf{v}$
- $f_i(\boldsymbol{\theta}) = M_d(\boldsymbol{\theta}, \mathbf{v}_i)$, deterministic generator associated with sample $\mathbf{v}_i \sim p(\mathbf{v})$
- $g_i(\boldsymbol{\theta}) = d(f_i(\boldsymbol{\theta}), \mathbf{y_0})$, distance of the generated data $f_i(\boldsymbol{\theta})$ from the observations
- $T(\mathbf{x}) : \mathbb{R}^{D_1} \rightarrow \mathbb{R}^{D_2}$ where $D_1 > D_2$, the mapping that computes the summary statistic
- $\mathbb{1}_{B_{d,\epsilon}(\mathbf{y_0})}(\mathbf{y})$, the indicator function; returns 1 if $d(\mathbf{y}, \mathbf{y_0}) \leq \epsilon$, else 0
- $L(\boldsymbol{\theta})$, the likelihood
- $L_{d,\epsilon}(\boldsymbol{\theta})$, the approximate likelihood

2 Background

2.1 Simulator-based models

As already stated at Chapter 1, in simulator-based models we cannot evaluate the posterior $p(\boldsymbol{\theta}|\mathbf{y_0}) \propto L(\boldsymbol{\theta})p(\boldsymbol{\theta})$, due to the intractability of the likelihood $L(\boldsymbol{\theta}) = p(\mathbf{y_0}|\boldsymbol{\theta})$. The following equation allows incorporating the simulator in the place of the likelihood and forms the basis of all likelihood-free inference approaches,

$$L(\boldsymbol{\theta}) = \lim_{\epsilon \to 0} c_\epsilon \int_{\mathbf{y} \in B_{d,\epsilon}(\mathbf{y_0})} p(\mathbf{y}|\boldsymbol{\theta}) d\mathbf{y} = \lim_{\epsilon \to 0} c_\epsilon \Pr(M_r(\boldsymbol{\theta}) \in B_{d,\epsilon}(\mathbf{y_0})) \tag{2.1}$$

where c_ϵ is a proportionality factor dependent on ϵ, needed when $\Pr(M_r(\boldsymbol{\theta}) \in B_{d,\epsilon}(\mathbf{y_0})) \to 0$, as $\epsilon \to 0$. Equation 2.1 describes that the likelihood of a specific parameter configuration $\boldsymbol{\theta}$ is proportional to the probability that the simulator will produce outputs equal to the observations, using this configuration.

2.1.1 Approximate Bayesian Computation (ABC) Rejection Sampling

ABC rejection sampling is a modified version of the traditional rejection sampling method, for cases when the evaluation of the likelihood is intractable. In the typical rejection sampling, a sample obtained from the prior $\boldsymbol{\theta} \sim p(\boldsymbol{\theta})$ gets accepted with probability $L(\boldsymbol{\theta})/\max_{\boldsymbol{\theta}} L(\boldsymbol{\theta})$. Though we cannot use this approach out-of-the-box (evaluating $L(\boldsymbol{\theta})$ is impossible in our case), we can modify the method incorporating the simulator.

In the discrete case scenario where $\mathbf{Y}_{\boldsymbol{\theta}}$ can take a finite set of values, the likelihood becomes $L(\boldsymbol{\theta}) = \Pr(\mathbf{Y}_{\boldsymbol{\theta}} = \mathbf{y_0})$ and the posterior $p(\boldsymbol{\theta}|\mathbf{y_0}) \propto \Pr(\mathbf{Y}_{\boldsymbol{\theta}} = \mathbf{y_0})p(\boldsymbol{\theta})$; hence, we can sample from the prior $\boldsymbol{\theta}_i \sim p(\boldsymbol{\theta})$, run the simulator $\mathbf{y}_i = M_r(\boldsymbol{\theta}_i)$ and accept $\boldsymbol{\theta}_i$ only if $\mathbf{y}_i = \mathbf{y_0}$.

The method above becomes less useful as the finite set of $\mathbf{Y}_{\boldsymbol{\theta}}$ values grows larger, since the probability of accepting a sample becomes smaller. In the limit where the set becomes infinite (i.e. continuous case) the probability becomes zero. In order for the method to work in this set-up, a relaxation is introduced; we relax the acceptance criterion by letting $\mathbf{y}_i$ lie in a larger set of points i.e. $\mathbf{y}_i \in B_{d,\epsilon}(\mathbf{y_0}), \epsilon > 0$. The region can be defined as $B_{d,\epsilon}(\mathbf{y_0}) := \{\mathbf{y} : d(\mathbf{y}, \mathbf{y_0}) \leq \epsilon\}$ where $d(\cdot, \cdot)$ can represent any valid distance. With this modification, the maintained samples follow the approximate posterior,

$$p_{d,\epsilon}(\boldsymbol{\theta}|\mathbf{y_0}) \propto Pr(\mathbf{y} \in B_{d,\epsilon}(\mathbf{y_0}))p(\boldsymbol{\theta}) \tag{2.2}$$

This method is called Rejection ABC.

2.1.2 Summary Statistics

When $\mathbf{y} \in \mathbb{R}^D$ lies in a high-dimensional space, generating samples inside $B_{d,\epsilon}(\mathbf{y_0})$ becomes rare even when ϵ is relatively large; this is the curse of dimensionality. As a representative example lets make the following hypothesis;

- d is set to be the Euclidean distance, hence $B_{d,\epsilon}(\mathbf{y_0}) := \{\mathbf{y} : ||\mathbf{y} - \mathbf{y_0}||_2^2 < \epsilon^2\}$ is a hyper-sphere with radius ϵ and volume $V_{hypersphere} = \frac{\pi^{D/2}}{\Gamma(D/2+1)}\epsilon^D$
- the prior $p(\boldsymbol{\theta})$ is a uniform distribution in a hyper-cube with side of length 2ϵ and volume $V_{hypercube} = (2\epsilon)^D$
- the generative model is the identity $\mathbf{y} = f(\boldsymbol{\theta}) = \boldsymbol{\theta}$

then the probability of drawing a sample inside the hypersphere equals the fraction of the volume of a hypersphere inscribed in a hypercube:

$$Pr(\mathbf{y} \in B_{d,\epsilon}(\mathbf{y_0})) = Pr(\boldsymbol{\theta} \in B_{d,\epsilon}(\mathbf{y_0})) = \frac{V_{hypersphere}}{V_{hypercube}} = \frac{\pi^{D/2}}{2^D\Gamma(D/2+1)} \to 0, \quad \text{as} \quad D \to \infty \tag{2.3}$$

We observe that the probability tends to 0, independently of ϵ; enlarging ϵ will not increase the acceptance rate. Intuitively, we can think that in high-dimensional spaces the volume of the hypercube concentrates at its corners. This generates the need for a mapping $T : \mathbb{R}^{D_1} \to \mathbb{R}^{D_2}$ where $D_1 > D_2$, for squeezing the dimensionality of the output. This dimensionality-reduction step, that redefines the area as $B_{d,\epsilon}(\mathbf{y_0}) := \{\mathbf{y} : d(T(\mathbf{y}), T(\mathbf{y_0})) \leq \epsilon\}$, is called *summary statistic* extraction, since the distance is not measured on the actual outputs, but on a summarisation (i.e. lower-dimension representation) of them.

2.1.3 Approximations introduced so far

So far, we have introduced some approximations for inferring the posterior as $p_{d,\epsilon}(\boldsymbol{\theta}|\mathbf{y_0}) \propto Pr(\mathbf{Y}_{\boldsymbol{\theta}} \in B_{d,\epsilon}(\mathbf{y_0}))p(\boldsymbol{\theta})$ where $B_{d,\epsilon}(\mathbf{y_0}) := \{\mathbf{y} : d(T(\mathbf{y}), T(\mathbf{y_0})) < \epsilon\}$. These approximations introduce two different types of errors:

- ϵ is chosen to be *big enough*, so that enough samples are accepted. This modification leads to the approximate posterior introduced in (2.2)

- T introduces some loss of information, making possible a $\mathbf{y}$ far away from the $\mathbf{y_0}$ i.e. $\mathbf{y} : d(\mathbf{y}, \mathbf{y_0}) > \epsilon$, to enter the acceptance region after the dimensionality reduction $d(T(\mathbf{y}), T(\mathbf{y_0})) \leq \epsilon$

In the following sections, we will not use the summary statistics in our expressions for the notation not to clutter. One could understand it as absorbing the mapping $T(\cdot)$ inside the simulator. In any case, all the propositions that will be expressed in the following sections are valid with the use of summary statistics.

2.1.4 Optimisation Monte Carlo (OMC)

Before we define the likelihood approximation as introduced in the OMC, approach lets define the indicator function based on $B_{d,\epsilon}(\mathbf{y})$. The indicator function $\mathbb{1}_{B_{d,\epsilon}(\mathbf{y})}(\mathbf{x})$ returns 1 if $\mathbf{x} \in B_{d,\epsilon}(\mathbf{y})$ and 0 otherwise. If $d(\cdot, \cdot)$ is a formal distance, due to symmetry $\mathbb{1}_{B_{d,\epsilon}(\mathbf{y})}(\mathbf{x}) = \mathbb{1}_{B_{d,\epsilon}(\mathbf{x})}(\mathbf{y})$, so the expressions can be used interchangeably.

$$\mathbb{1}_{B_{d,\epsilon}(\mathbf{y})}(\mathbf{x}) = \begin{cases} 1 & \text{if } \mathbf{x} \in B_{d,\epsilon}(\mathbf{y}) \\ 0 & \text{otherwise} \end{cases} \tag{2.4}$$

Likelihood approximation

Based on equation (2.2) and the indicator function as defined above (2.4), we can approximate the likelihood as:

$$L_{d,\epsilon}(\boldsymbol{\theta}) = \int_{\mathbf{y} \in B_\epsilon(\mathbf{y_0})} p(\mathbf{y}|\boldsymbol{\theta}) d\mathbf{y} = \int_{\mathbf{y} \in \mathbb{R}^D} \mathbb{1}_{B_{d,\epsilon}(\mathbf{y_0})}(\mathbf{y}) p(\mathbf{y}|\boldsymbol{\theta}) d\mathbf{y} \tag{2.5}$$

$$\approx \frac{1}{N} \sum_i^N \mathbb{1}_{B_{d,\epsilon}(\mathbf{y_0})}(\mathbf{y}_i), \text{ where } \mathbf{y}_i \sim M_r(\boldsymbol{\theta}) \tag{2.6}$$

$$\approx \frac{1}{N} \sum_i^N \mathbb{1}_{B_{d,\epsilon}(\mathbf{y_0})}(\mathbf{y}_i) \text{ where } \mathbf{y}_i = M_d(\boldsymbol{\theta}, \mathbf{v}_i), \mathbf{v}_i \sim p(\mathbf{v}) \tag{2.7}$$

This approach is quite intuitive; approximating the likelihood of a specific $\boldsymbol{\theta}$ requires sampling from the data generator and count the fraction of samples that lie inside the area around the observations. Nevertheless, by using the approximation of equation (2.6) we need to draw N new samples for each distinct evaluation of $L_{d,\epsilon}(\boldsymbol{\theta})$; this makes this approach quite inconvenient from a computational point-of-view. For this reason, we choose to approximate the integral as in equation (2.7); the nuisance variables are sampled once $\mathbf{v}_i \sim p(\mathbf{v})$ and we count the fraction of samples that lie inside the area using the deterministic simulators $M_d(\boldsymbol{\theta}, \mathbf{v}_i) \forall i$. Hence, the evaluation $L_{d,\epsilon}(\boldsymbol{\theta})$ for each different $\boldsymbol{\theta}$ does not imply drawing new samples all over again. Based on this approach, the unnormalised approximate posterior can be defined as:

$$p_{d,\epsilon}(\boldsymbol{\theta}|\mathbf{y_0}) \propto p(\boldsymbol{\theta}) \sum_i^N \mathbb{1}_{B_{d,\epsilon}(\mathbf{y_0})}(\mathbf{y}_i) \tag{2.8}$$

Further approximations for sampling and computing expectations

The posterior approximation in (2.2) does not provide any obvious way for drawing samples. In fact, the set $S_i = \{\boldsymbol{\theta} : M_d(\boldsymbol{\theta}, \mathbf{v}_i) \in B_{d,\epsilon}(\mathbf{y_0})\}$ can represent any arbitrary shape in the D-dimensional Euclidean space; it can be non-convex, can contain disjoint sets of $\boldsymbol{\theta}$ etc. This observation leads to the need for a further simplification of the posterior for being able to sample from it.

As a side-note, sampling could be performed in a straightforward fashion with importance sampling; using the prior as the proposal distribution $\boldsymbol{\theta}_i \sim p(\boldsymbol{\theta})$ and computing the weight as $w_i = \frac{L_{d,\epsilon}(\boldsymbol{\theta}_i)}{p(\boldsymbol{\theta}_i)}$. This approach has the same drawbacks as ABC rejection sampling; when the prior is wide or the dimensionality D is high, drawing a sample with non-zero weight is rare, leading to either poor Effective Sample Size (ESS) or huge execution time.

The OMC proposes a quite drastic simplification of the posterior; it squeezes all regions S_i into a single point $\boldsymbol{\theta}_i^* \in S_i$ attaching a weight w_i proportional to the volume of S_i. For obtaining $\boldsymbol{\theta}_i^*$, a gradient based optimiser is used for minimising $g_i(\boldsymbol{\theta}) = d(\mathbf{y_0}, f_i(\boldsymbol{\theta}))$ and the estimation of the volume of S_i is done using the Hessian approximation $\mathbf{H}_i \approx \mathbf{J}_i^{*T} \mathbf{J}_i^*$, where $\mathbf{J}_i^*$ is the Jacobian matrix of $g_i(\boldsymbol{\theta})$ at $\boldsymbol{\theta}_i^*$. Hence,

$$p(\boldsymbol{\theta}|\mathbf{y_0}) \propto p(\boldsymbol{\theta}) \sum_i^N w_i \delta(\boldsymbol{\theta} - \boldsymbol{\theta}_i^*) \tag{2.9}$$

$$\boldsymbol{\theta}_i^* = \text{argmin}_{\boldsymbol{\theta}}\, g_i(\boldsymbol{\theta}) \tag{2.10}$$

$$w_i \propto \frac{1}{\sqrt{det(\mathbf{J}_i^{*T} \mathbf{J}_i^*)}} \tag{2.11}$$

The distribution (2.9) provides weighted samples automatically and an expectation can be computed easily with the following equation,

$$E_{p(\boldsymbol{\theta}|\mathbf{y_0})}[h(\boldsymbol{\theta})] = \frac{\sum_i^N w_i p(\boldsymbol{\theta}_i^*) h(\boldsymbol{\theta}_i^*)}{\sum_i^N w_i p(\boldsymbol{\theta}_i^*)} \tag{2.12}$$

2.2 Robust Optimisation Monte Carlo (ROMC) approach

The simplifications introduced by OMC, although quite useful from a computational point-of-view, they suffer from some significant failure modes:

- The whole acceptable region S_i, for each nuisance variable, shrinks to a single point $\boldsymbol{\theta}_i^*$; this simplification may add significant error when then the area S_i is relatively big.

- The weight w_i is computed using information from $\boldsymbol{\theta}_i^*$, i.e. the curvature of g_i at the point $\boldsymbol{\theta}_i^*$. This approach can introduce significant error when g_i is almost flat at $\boldsymbol{\theta}_i^*$, leading to a $\det(\mathbf{J}_i^{*T} \mathbf{J}_i^*) \rightarrow 0 \Rightarrow w_i \rightarrow \infty$, thus dominating the posterior.

- There is no way to solve the optimisation problem $\boldsymbol{\theta}_i^* = \text{argmin}_{\boldsymbol{\theta}}\, [g_i(\boldsymbol{\theta})]$ when g_i is not differentiable.

2.2.1 Sampling and computing expectation in ROMC

The ROMC approach resolves the aforementioned issues. Instead of collapsing the acceptance regions into single points, it tries to approximate them with a bounding box and then defines a uniform distribution over it.[4], which serves as the proposal distribution for importance sampling. If we define as q_i, the uniform distribution defined on the $i-th$ bounding box, weighted sampling is performed as:

$$\boldsymbol{\theta}_{ij} \sim q_i \tag{2.13}$$

$$w_{ij} = \frac{\mathbb{1}_{B_{d,\epsilon}(\mathbf{y_0})}(M_d(\boldsymbol{\theta}_{ij}, \mathbf{v}_i))p(\boldsymbol{\theta}_{ij})}{q(\boldsymbol{\theta}_{ij})} \tag{2.14}$$

Having defined the procedure for obtaining weighted samples, any expectation $E_{p(\boldsymbol{\theta}|\mathbf{y_0})}[h(\boldsymbol{\theta})]$, can be approximated as,

$$E_{p(\boldsymbol{\theta}|\mathbf{y_0})}[h(\boldsymbol{\theta})] \approx \frac{\sum_{ij} w_{ij} h(\boldsymbol{\theta}_{ij})}{\sum_{ij} w_{ij}} \tag{2.15}$$

2.2.2 Construction of the proposal region

In this section we will describe mathematically the steps needed for computing the proposal distributions q_i. There will be also presented a Bayesian optimisation alternative when gradients are not available.

Define and solve deterministic optimisation problems

For each set of nuisance variables $\mathbf{v}_i, i = \{1, 2, \dots, \dots, \dots, n_1\}$ a deterministic function is defined as $f_i(\boldsymbol{\theta}) = M_d(\boldsymbol{\theta}, \mathbf{v}_i)$. For constructing the proposal region, we search for a point $\boldsymbol{\theta}_* : d(f_i(\boldsymbol{\theta}_*), \mathbf{y_0}) < \epsilon$; this point can be obtained by solving the the following optimisation problem:

$$\min_{\boldsymbol{\theta}} \quad g_i(\boldsymbol{\theta}) = d(\mathbf{y_0}, f_i(\boldsymbol{\theta})) \tag{2.16a}$$

$$\text{subject to} \quad g_i(\boldsymbol{\theta}) \leq \epsilon \tag{2.16b}$$

We maintain a list of the solutions $\boldsymbol{\theta}_i^*$ of the optimisation problems. If for a specific set of nuisance variables $\mathbf{v}_i$, there is no feasible solution we add nothing to the list. The optimisation problem can be treated as unconstrained, accepting the optimal point $\boldsymbol{\theta}_i^* = \text{argmin}_{\boldsymbol{\theta}} g_i(\boldsymbol{\theta})$ only if $g_i(\boldsymbol{\theta}_i^*) < \epsilon$.

Gradient-based approach

The nature of the generative model $M_r(\boldsymbol{\theta})$, specifies the properties of the objective function g_i. If g_i is continuous with smooth gradients $\nabla_{\boldsymbol{\theta}} g_i$ any gradient-based iterative algorithm can be used for solving 2.16a. The gradients $\nabla_{\boldsymbol{\theta}} g_i$ can be either provided in closed form or be approximated by finite differences.

Bayesian optimisation approach

In cases where the gradients are not available, the Bayesian optimisation scheme provides an alternative choice (Shahriari et al. 2016). With this approach, apart from obtaining an optimal $\boldsymbol{\theta}_i^*$, a surrogate model $\hat{d}_i$ of the distance g_i is fitted; this approximate model can be used in the following steps for making the method more efficient. Specifically, in the construction of the proposal region and in equations (2.2), (2.13), (2.15) it could replace g_i in the evaluation of the indicator function, providing a major speed-up.

[4] The description on how to estimate the bounding box is provided in the following chapters.

Construction of the proposal area q_i

After obtaining a $\boldsymbol{\theta}_i^*$ such that $g_i(\boldsymbol{\theta}_i^*) < \epsilon$, we need to construct a bounding box around it. The bounding box must contain the acceptance region around $\boldsymbol{\theta}_i^*$, i.e. $\{\boldsymbol{\theta} : g_i(\boldsymbol{\theta}) < \epsilon \text{ and } d(\boldsymbol{\theta}, \boldsymbol{\theta}_i^*) < M\}$. The second condition $d(\boldsymbol{\theta}, \boldsymbol{\theta}_i^*) < M$ is meant to describe that if $S_i := \{\boldsymbol{\theta} : g_i(\boldsymbol{\theta}) < \epsilon\}$ contains a number of disjoint sets of $\boldsymbol{\theta}$ that respect $g_i(\boldsymbol{\theta}) < \epsilon$, we want our bounding box to fit only the one that contains $\boldsymbol{\theta}_i^*$. We seek for a bounding box that is as tight as possible to the local acceptance region (enlarging the bounding box without a reason decreases the acceptance rate) but large enough for not discarding accepted areas.

In contrast with the OMC approach, we construct the bounding box by obtaining search directions and querying the indicator function as we move on them. The search directions $\mathbf{v}_d$ are computed as the eigenvectors of the curvature at $\boldsymbol{\theta}_i^*$ and a line-search method is used to obtain the limit point where $g_i(\boldsymbol{\theta}_i^* + \kappa \mathbf{v}_d) \geq \epsilon$[5]. The Algorithm 3 describes the method in-depth. After the limits are obtained along all search directions, we define bounding box and the uniform distribution q_i. This is the proposal distribution used for the importance sampling as explained in (2.13).

2.3 Algorithmic description of ROMC

In this section, we will provide the algorithmic description of the ROMC method; how to solve the optimisation problems using either the gradient-based approach or the Bayesian optimisation alternative and the construction of the bounding box. Afterwards, we will discuss the advantages and disadvantages of each choice in terms of accuracy and efficiency.

At a high-level, the ROMC method can be split into the training and the inference part.

Training part

At the training (fitting) part, the goal is the estimation of the proposal regions q_i. The tasks are (a) sampling the nuisance variables $\mathbf{v}_i \sim p(\mathbf{v})$ (b) defining the optimisation problems $\min_{\boldsymbol{\theta}} g_i(\boldsymbol{\theta})$ (c) obtaining $\boldsymbol{\theta}_i^*$ (d) checking whether $d_i^* \leq \epsilon$ and (e) building the bounding box for obtaining the proposal region q_i. If gradients are available, using a gradient-based method is advised for obtaining $\boldsymbol{\theta}_i^*$ much faster. Providing $\nabla_{\boldsymbol{\theta}} g_i$ in closed-form provides an upgrade in both accuracy and efficiency; If closed-form description is not available, approximate gradients with finite-differences requires two evaluations of g_i for **every** parameter $\boldsymbol{\theta}_d$, which works adequately well for low-dimensional problems. When gradients are not available or g_i is not differentiable, the Bayesian optimisation paradigm exists as an alternative solution. In this scenario, the training part becomes slower due to fitting of the surrogate model and the blind optimisation steps. Nevertheless, the subsequent task of computing the proposal region q_i becomes faster since $\hat{d}_i$ can be used instead of g_i; hence we avoid to run the simulator $M_d(\boldsymbol{\theta}, \mathbf{v}_i)$ for each query. The algorithms 1 and 2 present the above procedure.

Inference Part

Performing the inference includes one or more of the following three tasks; (a) evaluating the unnormalised posterior $p_{d,\epsilon}(\boldsymbol{\theta}|\mathbf{y_0})$ (b) sampling from the posterior $\boldsymbol{\theta}_i \sim p_{d,\epsilon}(\boldsymbol{\theta}|\mathbf{y_0})$ (c) computing an expectation $E_{\boldsymbol{\theta}|\mathbf{y_0}}[h(\boldsymbol{\theta})]$. Computing an expectation can be done easily after weighted samples are obtained using the equation 2.15, so we will not discuss it separately.

Evaluating the unnormalised posterior requires solely the deterministic functions g_i and the prior distribution $p(\boldsymbol{\theta})$; there is no need for solving the optimisation problems and building the proposal regions. The evaluation requires iterating over all g_i and evaluating the distance from the observed data. In contrast, using the GP approach, the optimisation part should be performed first for fitting the surrogate models $\hat{d}_i(\boldsymbol{\theta})$ and evaluate the indicator function on them. This provides an important speed-up, especially when running the simulator is computationally expensive.

Sampling is performed by getting n_2 samples from each proposal distribution q_i. For each sample $\boldsymbol{\theta}_{ij}$, the indicator function is evaluated $\mathbb{1}_{B^i_{d,\epsilon}(\mathbf{y_0})}(\boldsymbol{\theta}_{ij})$ for checking if it lies inside the acceptance region. If

[5] $-\kappa$ is used as well for the opposite direction along the search line

so the corresponding weight is computed as in (2.13). As before, if a surrogate model $\hat{d}$ is available, it can be utilised for evaluating the indicator function. At the sampling task, the computational benefit of using the surrogate model is more valuable compared to the evaluation of the posterior, because the indicator function must be evaluated for a total of $n_1 \times n_2$ points. The sampling algorithms are presented step-by-step in algorithms 4 and 5.

In summary, we can state that the choice of using a Bayesian optimisation approach provides a significant speed-up in the inference part with the cost of making the training part slower and a possible approximation error. It is typical in many Machine-Learning use cases, being able to provide enough time and computational resources for the training phase, but asking for efficiency in the inference part.

Algorithm 1 Training Part - Gradient approach. Requires $g_i(\boldsymbol{\theta}), p(\boldsymbol{\theta})$

```
1: for $i \leftarrow 1$ to $n$ do
2:     Obtain $\boldsymbol{\theta}_i^*$ using a Gradient Optimiser
3:     if $g_i(\boldsymbol{\theta}_i^*) > \epsilon$ then
4:         go to 1
5:     else
6:         Approximate $\mathbf{J}_i^* = \nabla g_i(\theta)$ and $H_i \approx \mathbf{J}_i^T \mathbf{J}_i$
7:         Use Algorithm 3 to obtain $q_i$
   return $q_i, p(\theta), g_i(\theta)$
```

Algorithm 2 Training Part - GP approach. Requires $g_i(\theta), p(\theta)$

```
1: for $i \leftarrow 1$ to $n$ do
2:     Obtain $\theta_i^*, \hat{d}_i(\theta)$ using a GP approach
3:     if $g_i(\theta_i^*) > \epsilon$ then
4:         go to 1
5:     else
6:         Approximate $H_i \approx \mathbf{J}_i^T \mathbf{J}_i$
7:         Use Algorithm 3 to obtain $q_i$
   return $q_i, p(\theta), \hat{d}_i(\theta)$
```

Algorithm 3 Computation of the proposal distribution q_i; Needs, a model of distance d, optimal point $\boldsymbol{\theta}_i^*$, number of refinements K, step size η and curvature matrix $\mathbf{H}_i$ ($\mathbf{J}_i^T \mathbf{J}_i$ or GP Hessian)

```
1: Compute eigenvectors $\mathbf{v}_d$ of $\mathbf{H}_i$ $(d = 1, \dots, ||\boldsymbol{\theta}||)$
2: for $d \leftarrow 1$ to $||\boldsymbol{\theta}||$ do
3:     $\tilde{\boldsymbol{\theta}} \leftarrow \boldsymbol{\theta}_i^*$
4:     $k \leftarrow 0$
5:     repeat
6:         repeat
7:             $\tilde{\boldsymbol{\theta}} \leftarrow \tilde{\boldsymbol{\theta}} + \eta\ \mathbf{v}_d$          ▷ Large step size $\eta$.
8:         until $d(f_i(\tilde{\boldsymbol{\theta}}), \mathbf{y_0}) > \epsilon$
9:         $\tilde{\boldsymbol{\theta}} \leftarrow \tilde{\boldsymbol{\theta}} - \eta\ \mathbf{v}_d$
10:        $\eta \leftarrow \eta/2$          ▷ More accurate region boundary
11:        $k \leftarrow k + 1$
12:    until $k = K$
13:    Set final $\tilde{\boldsymbol{\theta}}$ as region end point.
14:    Repeat steps 3 - 13 for $\mathbf{v}_d = -\mathbf{v}_d$
15: Fit a rectangular box around the region end points and define $q_i$ as uniform distribution
```

Algorithm 4 Sampling - Gradient Based approach. Requires $g_i(\theta), p(\theta), q_i$

```
1: for $i \leftarrow 1$ to $n_1$ do
2:     for $j \leftarrow 1$ to $n_2$ do
3:         $\theta_{ij} \sim q_i$
4:         if $g_i(\theta_{ij}) > \epsilon$ then
5:             Reject $\theta_{ij}$
6:         else
7:             $w_{ij} = \frac{p(\theta_{ij})}{q(\theta_{ij})}$
8:             Accept $\theta_{ij}$, with weight $w_{ij}$
```

Algorithm 5 Sampling - GP approach. Requires $\hat{d}_i(\theta), p(\theta), q_i$

```
1: for $i \leftarrow 1$ to $n_1$ do
2:     for $j \leftarrow 1$ to $n_2$ do
3:         $\theta_{ij} \sim q_i$
4:         if $\hat{d}_i(\theta_{ij}) > \epsilon$ then
5:             Reject $\theta_{ij}$
6:         else
7:             $w_{ij} = \frac{p(\theta_{ij})}{q(\theta_{ij})}$
8:             Accept $\theta_{ij}$, with weight $w_{ij}$
```

2.4 Engine for Likelihood-Free Inference (ELFI) package

!!NOT fully written, I have to add some more info!!

The Engine for Likelihood-Free Inference (ELFI) Lintusaari et al. 2018 is a Python software library dedicated to likelihood-free inference (LFI). ELFI models in a convenient manner all the fundamental components of a Probabilistic Model such as priors, simulators, summaries and distances. Furthermore, in the ELFI there are implemented a wide range of likelihood-free inference methods.

2.4.1 Modelling

ELFI models the Probabilistic Model as Directed Acyclic Graph (DAG); it implements this functionality based on the package NetworkX, which is designed for creating general purpose graphs. Although not restricted to that, in most cases the structure of a likelihood-free model follows the pattern presented in figure 4; there are edges that connect the *prior* distributions to the simulator, the simulator is connected to the summary statistics which are connected to the distance, which is the output node. Samples can be obtained from all nodes through sequential sampling. The nodes that are defined as *elfi.Prior*[6] are automatically considered as the parameters of interest and they are the only nodes that should provide pdf evaluation, apart from sampling. The function passed as argument in the *elfi.Summary* node can be any valid Python function with arguments the prior variables.

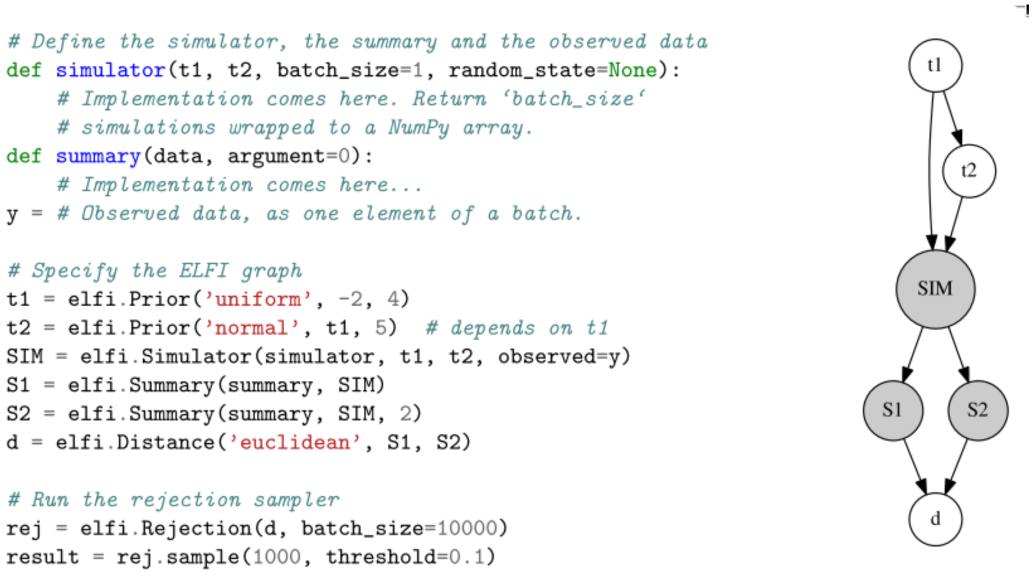

```python
# Define the simulator, the summary and the observed data
def simulator(t1, t2, batch_size=1, random_state=None):
    # Implementation comes here. Return ‘batch_size‘
    # simulations wrapped to a NumPy array.
def summary(data, argument=0):
    # Implementation comes here...
y = # Observed data, as one element of a batch.

# Specify the ELFI graph
t1 = elfi.Prior('uniform', -2, 4)
t2 = elfi.Prior('normal', t1, 5)  # depends on t1
SIM = elfi.Simulator(simulator, t1, t2, observed=y)
S1 = elfi.Summary(summary, SIM)
S2 = elfi.Summary(summary, SIM, 2)
d = elfi.Distance('euclidean', S1, S2)

# Run the rejection sampler
rej = elfi.Rejection(d, batch_size=10000)
result = rej.sample(1000, threshold=0.1)
```

Figure 2: Image taken from Lintusaari et al. 2018

2.4.2 Inference Methods

All Inference Methods that are implemented in ELFI, follow some common guidelines; (a) their initialisation should by defined by passing the output graph as the initial argument and afterwards come the rest hyper-parameters of the method and (b) they must provide a basic inference functionality, e.g. *<method>.sample()*, which returns a predefined *elfi.Result* object containing the obtained samples along with some other useful functionalities (e.g. plotting the marginal posteriors).

A good collection of likelihood-free inference methods is implemented so far, such as the *ABC Rejection Sampler* and *Sequential Monte Carlo ABC Sampler*. A quite central method implemented by ELFI is the *Bayesian Optimisation for Likelihood-Free Inference (BOLFI)*, which is methodologically quite close to the ROMC method we implement in the current dissertation.

[6] The *elfi.Prior* functionality is a wrapper around the scipy.stats package.

3 Implementation

In this chapter, we will exhibit the implementation of the ROMC inference method at the ELFI package. The presentation is split into two logical blocks; In Sections 3.1, 3.2, 3.3, 3.4 we present the functionalities provided by our implementation, from the **user's point-of-view**. These sections demonstrate how a practitioner could use our ROMC implementation for performing the inference in a real-case scenario. For providing a practical overview of the implementation, we set-up a simple running example and illustrate the functionalities on top of it. In contrast, in the final Section 3.5 we delve into the internals of the code, presenting all the tiny details of the implementation. This Section mainly refers to a **developer or a researcher** who would like to use ROMC as a meta-algorithm and experiment with novel approaches for solving specific tasks. We have designed our implementation preserving extensibility and customisation; hence, a researcher may intervene in parts of the method without too much effort. This Section can serve as a driver for achieving so.

3.1 General Design

In figure 4 we present an overview of our implementation; one could think of figure 4 as a depiction of the main class of our implementation, which is called ROMC, while the entities inside the green and blue ellipses are the main functions of the class. Following the common naming principles, the methods starting with an underscore (green ellipses) represent internal (private) functions and are not meant to be used by a user, whereas the rest of the methods (blue ellipses) are the functionalities used for performing the inference.As mentioned before, the implementation favours extensibility; the building blocks that compose the method have been designed in an isolated fashion so that a practitioner may replace them without the method to collapse.

Figure 4 groups the ROMC implementation into the training, the inference and the evaluation part, following the arrangement used in the algorithmic presentation (section 2.3). The training part includes all the steps until the computation of the proposal regions; sampling the nuisance variables, defining the optimisation problems, solving them and constructing the regions. The inference part comprises of evaluating the unnormalised posterior (and the normalised one, in low-dimensional cases), sampling and computing an expectation. Moreover, the ROMC implementation provides some utilities for inspecting the training process, such as plotting the histogram of the distances $d_i^* = g_i(\theta_i^*)$, $\forall i \in \{1, \ldots, n_1\}$ after solving the optimisation problems and visualising the constructed bounding box[7]. Finally, there are implemented two functionalities for evaluating the inference; (a) computing the Effective Sample Size (ESS) of the obtained weighted samples and (b) measuring the divergence of the approximate posterior from the ground-truth, if the latter is available.[8]

Simple 1D example

For illustrating the implemented functionalities, we choose the following $1D$ as as in Ikonomov and Gutmann 2019; the prior distribution is the uniform in the range $[-2.5, 2.5]$, i.e. $p(\theta) = \mathcal{U}(\theta; -2.5, 2.5)$ and the generative model is the following,

$$p(y|\theta) = \begin{cases} \theta^4 + u & \text{if } \theta \in [-0.5, 0.5] \\ |\theta| - c + u & \text{otherwise} \end{cases} \tag{3.1}$$

where $u \sim \mathcal{N}(0,1)$. There is only one observation $y_0 = 0$. In this example, the likelihood can be evaluated quite easily, hence it can be solved quite easily without a likelihood-free inference model. This is quite convenient at this point, since apart from illustrating the functionalities, we can quite easily validate the inference. The ground-truth posterior of the example is shown in figure 3.

The corresponding *elfi* code for building the specific generative model is the following.

[7] if the parametric space is up to $2D$

[8] Normally, the ground-truth posterior is not available; that is the meaning of performing the inference! Though this functionality is useful in cases where the posterior can be computed numerically or with an alternative method (i.e. ABC Rejection Sampling) and we would like to measure the discrepancy between the two approximations.

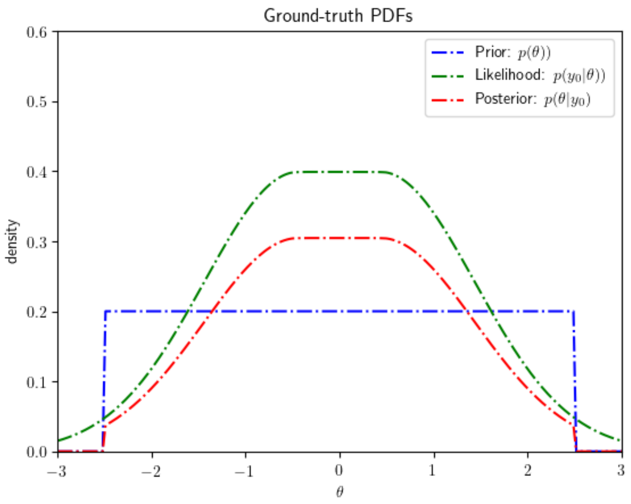

Figure 3: Ground-truth posterior distribution for our simple 1D example

ELFI code for modelling the example

In the following code snippet, we model the simple example in the ELFI package. We observe that the initialisation of the ROMC inference method is quite intuitive; we juct pass the distance node of the simulator as the first argument. The arguments `left_lim, right_lim` which represent the limits of the prior distribution are optional; they are needed only if `romc.eval_posterior()` is called in the inference part, for approximating the partition.

```
import elfi
import scipy.stats as ss
import numpy as np

def simulator(t1, batch_size=1,random_state=None):
    if t1 < -0.5:
        y = ss.norm(loc=-t1-c, scale=1).rvs(random_state=random_state)
    elif t1 <= 0.5:
        y = ss.norm(loc=t1**4, scale=1).rvs(random_state=random_state)
    else:
        y = ss.norm(loc=t1-c, scale=1).rvs(random_state=random_state)
    return y

# observation
y = 0

# Elfi graph
t1 = elfi.Prior('uniform', -2.5, 5)
sim = elfi.Simulator(simulator, t1, observed=y)
d = elfi.Distance('euclidean', sim)

# Define ROMC inference method
left_lim = np.array([-2.5])
right_lim = np.array([2.5])
romc = elfi.ROMC(d, left_lim=left_lim, right_lim=right_lim)
```

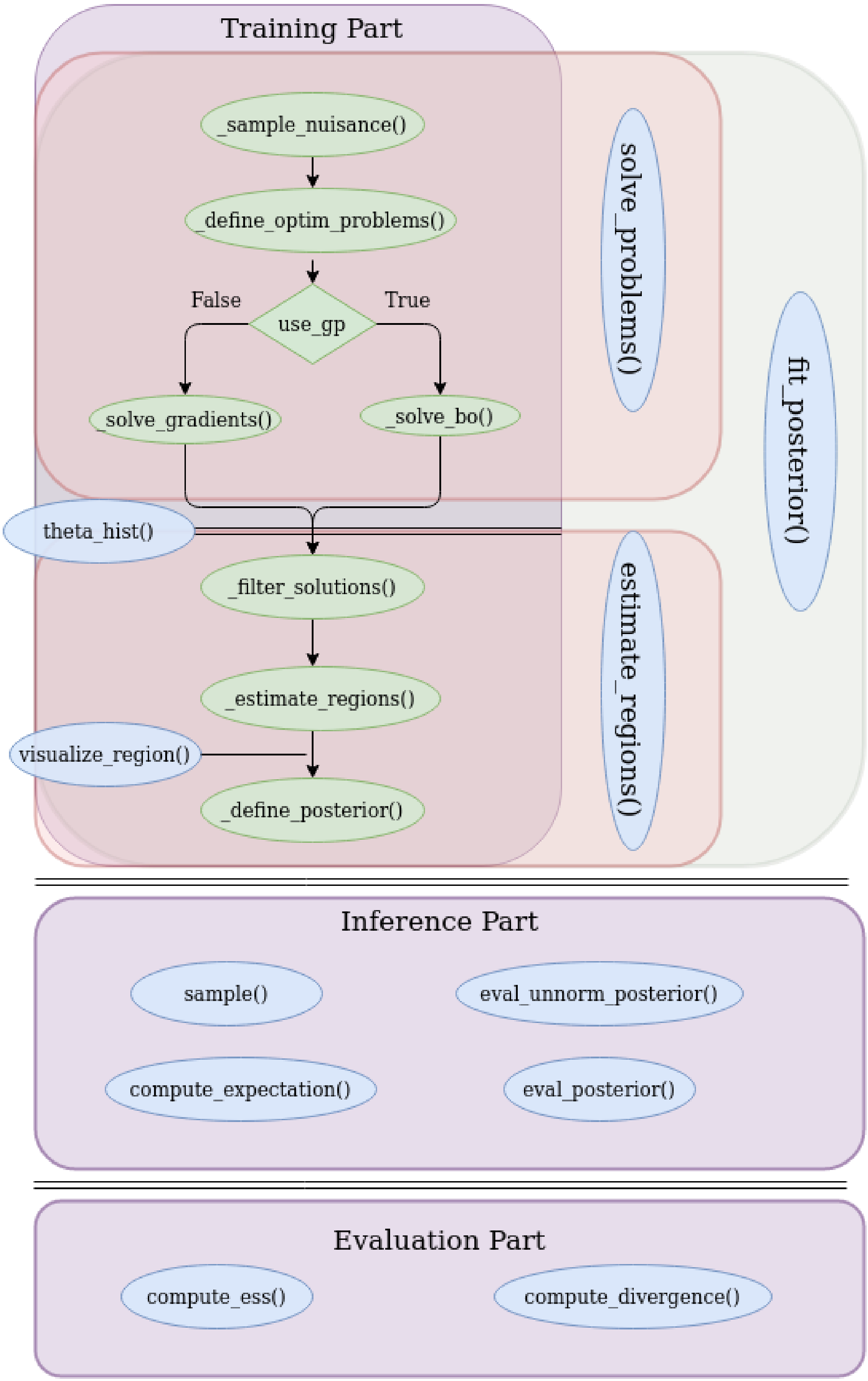

Figure 4: Overview of the ROMC implementation. The training part follows a sequential pattern; the functions in the green ellipses must be called in a sequential fashion for completing the training part and define the posterior distribution. The functions in blue ellipses are the functionalities provided to the user.

3.2 Training

The training part contains the 6 following functionalities:

- `romc.solve_problems(n1, seed=None, use_bo=False)`
- `romc.estimate_regions(eps)`
- `romc.theta_hist(**kwargs)`
- `romc.visualize_region(i)`
- `romc.compute_eps(quantile)`
- `romc.fit_posterior(n1, eps, quantile=None, use_bo=False, seed=None)`

Function (i): `romc.solve_problems(n1, seed=None, use_bo=False)`

This routine is responsible for (a) drawing the nuisance variables, (b) define the optimisation problems and (c) solve them using either a gradient-based optimiser or Bayesian optimisation. The aforementioned tasks are done in a sequential fashion, as show in figure 4. The defininition of the optimisation problems is performed by drawing n_1 integer numbers from a discrete uniform distribution $u_i \sim \mathcal{U}\{1, 2^{32} - 1\}$. Each integer u_i is the seed used in ELFI's random simulator. Hence from a programmatistic point-of-view drawing the state of all random variables $\mathbf{v}_i$ as described in the previous chapter, traces back to just setting the seed that initialises the state of the pseudo-random generator, before asking a sample from the simulator.

Finally, passing an integer number as the argument `seed` absorbs all the randomness of the optimistation part (e.g. drawing initial points for the optimisation procedure), making the whole process reproducible.

Setting the argument `use_bo=True`, chooses the Bayesian Optimisation scheme for obtaining θ_i^*. In this case the function $g_i(\boldsymbol{\theta}) = d(M_d(\boldsymbol{\theta}, \mathbf{v} = \mathbf{v}_i))$ which by default is evaluated using the simulator, is replaced by a Gaussian Proccess surrogate model $\hat{d}$, which is used in all next steps.

Function (ii): `romc.theta_hist(**kwargs)`

This function can serve as an intermediate step of manual inspection, for helping the user choose which threshold ϵ to use. It plots a histogram of the distances at the optimal point $g_i(\boldsymbol{\theta}_i^*) : \{i = 1, 2, \ldots, n_1\}$ or d_i^* in case `use_bo=True`. The function accepts all keyword arguments and forwards them to the underlying `matplotlib.hist()` function; in this way the user may customize some properties of the histogram, such as the number of bins or the range of values.

Function (iii): `romc.compute_eps(quantile)`

This function return the appropriate distance value $d^*_{i=\kappa}$ where $\kappa = \lfloor \frac{quantile}{n} \rfloor$ from the collection $\{d_i^*\} \forall i = \{1, \ldots, n\}$ where n is the number of accepted solutions. It can be used to automate the selection of the threshold ϵ, e.g. `eps=romc.compute_eps(quantile=0.9)`.

Function (iv): `romc.estimate_regions(eps)`

This function constructs the bounding boxes around the optimal points $\boldsymbol{\theta}_i^* : i = 1, 2, \ldots, n_1$ following the Algorithm 3. The Hessian matrix is approximated based on the Jacobian $\mathbf{H}_i = \mathbf{J}_i^T \mathbf{J}_i$. The eigenvectores are computed using the function `numpy.linalg.eig()` that calls, under the hood, the `_geev LAPACK`. A check is performed so that the matrix $\mathbf{H}_i$ is not singular; if this is the case, the eigenvectors are set to be the vectors of the orthonormal basis. Afterwards, the limits are obtained by repeteadly querying the distance function ($g_i(\boldsymbol{\theta})$ or $\hat{d}(\boldsymbol{\theta})$) along the search directions. In section 3.5, we provide some details regarding the way the bounding box is defined as a class and sampling is performed on it.

Function (v): `romc.fit_posterior(n1, eps, quantile=None, use_bo=False, seed=None)`

This function merges all steps for constructing the bounding box into a single command. If the user doesn't want to manually inspect the histogram of the distances before deciding where to set the threshold ϵ, he may call `romc.fit_posterior()` and the whole training part will be done end-to-end. There are two alternatives for setting the threshold ϵ; the first is to set to a specific value blindly and the second is to set at as a specific quantile of the histogram of distances. In the second scenario the `quantile` argument must be set to a floating number in the range $[0, 1]$ and `eps='auto'`.

Function (vi): `romc.visualize_region(i)`

It can be used as an inspection utility for cases where the parametric space is up to two dimensional. The argument `i` is the index of the corresponding optimization problem i.e. $i < n_1$.

Example

Here we will illustrate the aforementioned functionalities using the simple 1D example we set up in the previous chapter. The following code snippet performs the training part at ELFI.

```
n1 = 500
seed = 21
eps = .75
use_bo = False # True, if using Bayesian optimisation

# Training set-by-step
romc.solve_problems(n1=n1, seed=seed, use_bo=use_bo)
romc.theta_hist(bins=100)
romc.estimate_regions(eps=eps)
romc.visualize_region(i=1)

# Equivalent one-line command
# romc.fit_posterior(n1=n1, eps=eps, use_bo=use_bo, seed=seed)
```

As stated before, switching to the Bayesian optimisation scheme needs nothing more the setting the argument `use_bo=True`; all the following command remain unchanged. In figure 8 we illustrate the distribution of the distances obtained and the acceptance area of the first optimisation problem. We observe that most optimal points produce almost zero distance.

3.3 Performing the Inference

The inference part contains the 4 following functionalities:

- `romc.sample(n2, seed=None)`
- `romc.eval_unnorm_posterior(theta)`
- `romc.eval_posterior(theta)`
- `romc.compute_expectation(h)`

Function (i): `romc.sample(n2)`

This is the basic inference utility of the ROMC implementation. The samples are drawn from a uniform distribution q_i defined over the corresponding bounding box and the weight w_i is computed as in equation (2.13). The function stores an `elfi.Result` object as `romc.result` attribute. The

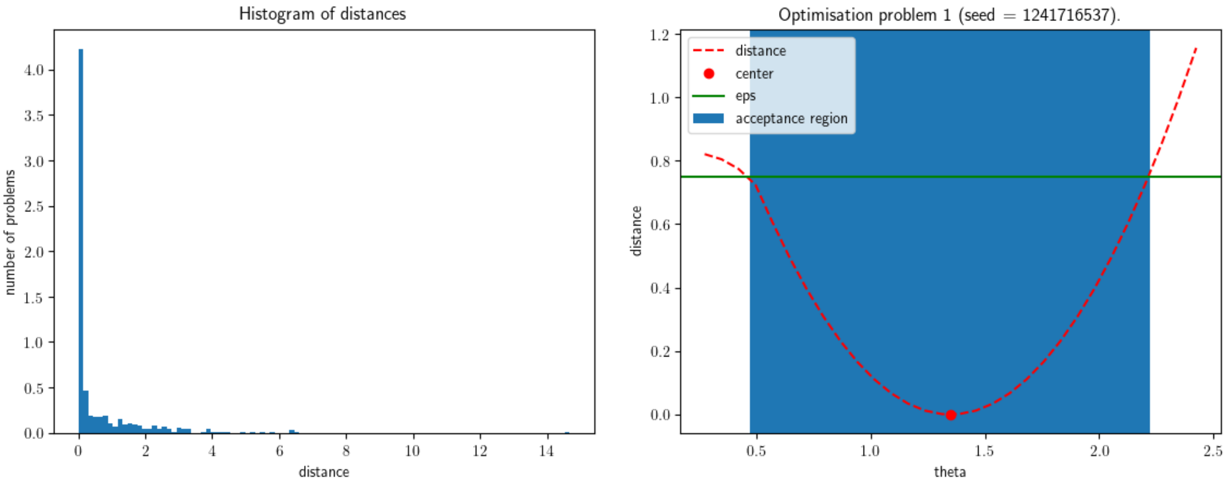

Figure 5: Histogram of distances and visualisation of a specific region.

`elfi.Result` provides by some usefull functionalities for inspecting the obtained samples such as `romc.result.summary()` that prints the number. A comlete overview of these functionalities is provided in ELFI's official documentation.

Function (ii):nn `romc.compute_expectation(h)`

This function computes the expectation $E_{p(\boldsymbol{\theta}|\mathbf{y_0})}[h(\boldsymbol{\theta})]$ using the expression (2.15). The argument `h` can be any python `Callable` that accepts a one-dimensional `np.ndarray` as input and returns a one-dimensional `np.ndarray` as output.

Function (iii): `romc.eval_unorm_posterior(theta)`

This function computes the unnormalised posterior approximation using the expression (2.2).

Function (iv): `romc.eval_posterior(theta)`

This function evaluates the normalised posterior. For doing so it needs to approximate the partition function $Z = \int_{\boldsymbol{\theta}:p(\boldsymbol{\theta})>0} p_{d,\epsilon}(\boldsymbol{\theta}|\mathbf{y_0})d\boldsymbol{\theta}$; this is done using the Riemann integral aproximation. Unfortunatelly, the Riemann approximation does not scale well in high-dimensional spaces, hence the approximation is tractable only at low-dimensional parametric spaces. Given that this functionality is particulary useful for ploting the posterior, we could say that it is meaningful to be used for up to $3D$ parametric spaces, even though it is not restricted to that. Finally, for this functionality to work, the left and right limit determinining a bounding box that includes the area where the prior distribution has mass must have been passed as the `left_lim, right_lim` in the initialisation of the `elfi.ROMC` object.

Example - Sampling and compute expectation

With the following code snippet, we perform weighted sampling from the ROMC approximate posterior. Afterwards, we used some ELFI's built-in tools to get a summary of the obtained samples. In figure 6, we observe the histogram of the weighted samples and the acceptance region of the first deterministic function (as before) alongside with the obtained samples obtained from it. Finally, in the code snippet we demonstrate how to use the `compute_expectation` function; in the current example we define `h` in order to compute firstly the empirical mean and afterwards the empirical variance. In both cases, the empirical result is close to the ground truth $\mu = 0$ and $\sigma^2 = 1$.

```
seed = 21
n2 = 50
romc.sample(n2=n2, seed=seed)

# visualize region, adding the samples now
romc.visualize_region(i=1)

# Visualise marginal (built-in ELFI tool)
romc.result.plot_marginals(weights=romc.result.weights, bins=100, range=(-3,3))

# Summarize the samples (built-in ELFI tool)
romc.result.summary()
# Number of samples: 1720
# Sample means: theta: -0.0792

# compute expectation
print("Expected value    : %.3f" % romc.compute_expectation(h=lambda x: np.squeeze(x)))
# Expected value    : -0.079

print("Expected variance: %.3f" % romc.compute_expectation(h=lambda x: np.squeeze(x)**2))
# Expected variance: 1.061
```

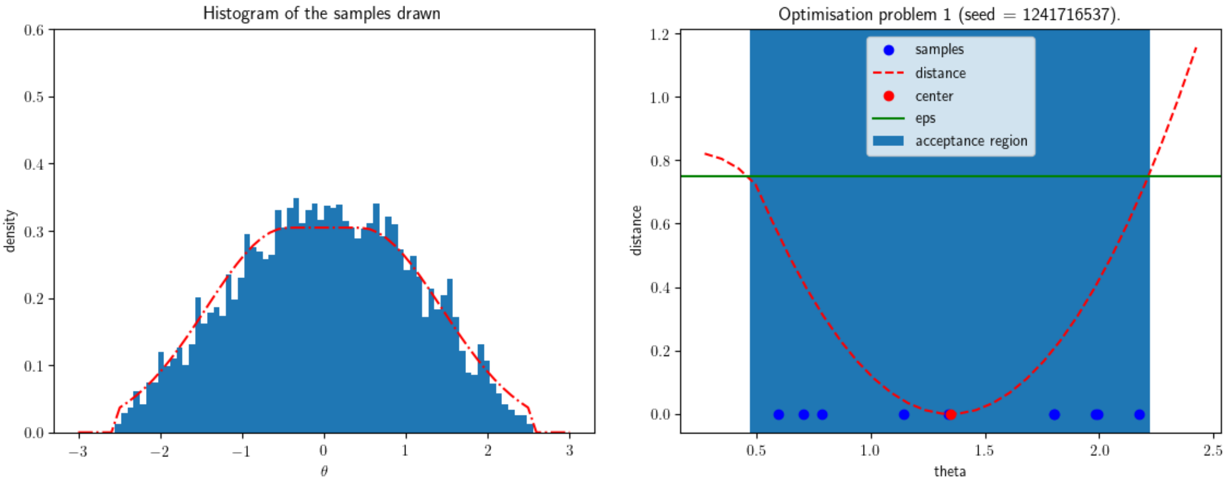

Figure 6: (a) Left: Histogram of the obtained samples. (b) Right: Acceptance region around θ_1^* with the obtained samples ploted inside.

Example - Evaluate Posterior

The `romc.eval_unnorm_posterior(theta)` evaluates the posterior at point θ using the expression (2.8). The `romc.eval_posterior(theta)` approximates the partition function $Z = \int_{\boldsymbol{\theta}} p_{d,\epsilon}(\boldsymbol{\theta}|\mathbf{y_0}) d\boldsymbol{\theta}$ using the Riemann approximation in the points where the prior has mass; hence it doesn't scale well to high-dimensional spaces. In our simple example, this utility can provide a nice plot of the approximate posterior as illustrated in figure 7. We observe that the approximation is quite close to the ground-truth posterior.

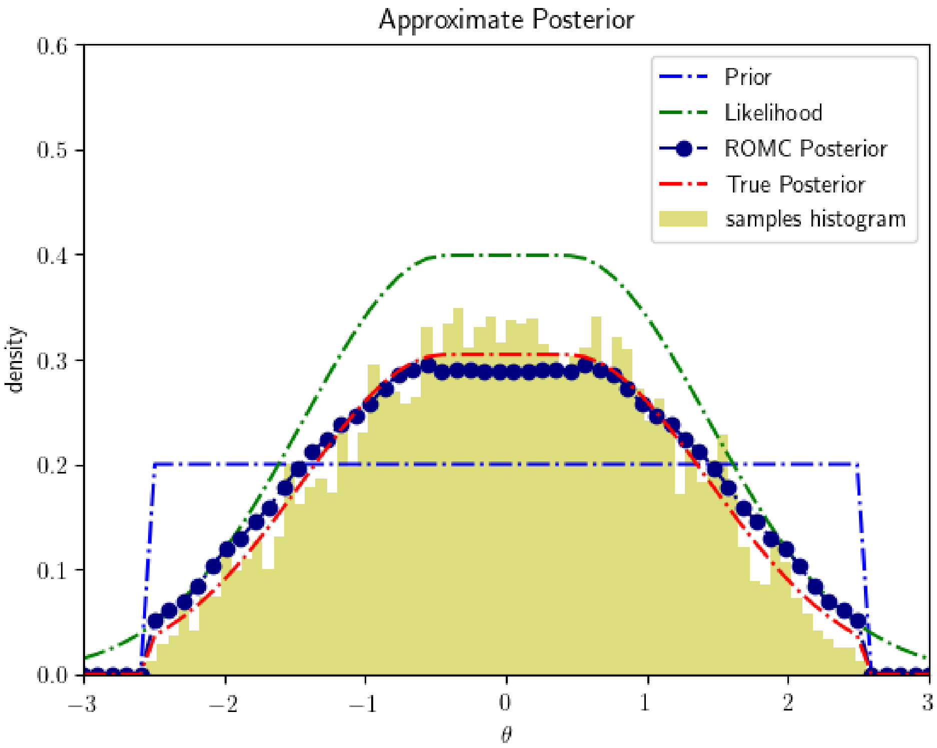

Figure 7: Approximate posterior evaluation.

3.4 Evaluation

The ROMC implementation provides two functions for evaluating the inference results,

- `romc.compute_divergence(gt_posterior, step=0.1, distance="Jensen-Shannon")`
- `romc.compute_ess()`

The `romc.compute_divergence(gt_posterior, step=0.1, distance="Jensen-Shannon")`

Function (i): `romc.compute_divergence(theta)`

This function computes the divergence between the ROMC approximation and the ground truth posterior. Since the compuation of the divergence is performed using the Riemann approximation in can only work in low dimensional parametric spaces; it is suggested to be used for up to a $3D$ parametric space.As mentioned in the beginning of this chapter, in a real-case scenario it is not expected the ground-truth posterior to be available; this is the whole meaning of performing the inference. However, there are two scenarios where this functionality can be useful; (a) when the likelihood is tractable and we want to check the accuracy of the ROMC method (as in the running-example) (b) when we want to compute the divergence between the ROMC's posterior approximation and another approximation e.g. ABC Rejection. The argument `step` defines step used in the Riemann approximation and the argument `distance` can take either the `Jensen-Shannon` or the `KL-divergence` value, for computing the appropriate distance.

Function (ii): `romc.compute_ess()`

This function compute the Effective Sample Size (ESS) using the following expression,

$$ESS = \frac{(\sum_i w_i)^2}{\sum_i w_i^2} \tag{3.2}$$

```
res = romc.compute_divergence(wrapper, distance="Jensen-Shannon")
print("Jensen-Shannon divergence: %.3f" % res)
# Jensen-Shannon divergence: 0.025

print("Nof Samples: %d, ESS: %.3f" % (len(romc.result.weights), romc.compute_ess()))
# Nof Samples: 19950, ESS: 16694.816
```

3.5 Implementation details for developers

!! NOT DONE YET !! Here I will analyse the internals of the implemntation and I will explain how the implementation hepls extensibility. I will also explain how a practiotioner may use ROMC as meta-algotrithm and use his custom methods as part of the inference procedure.

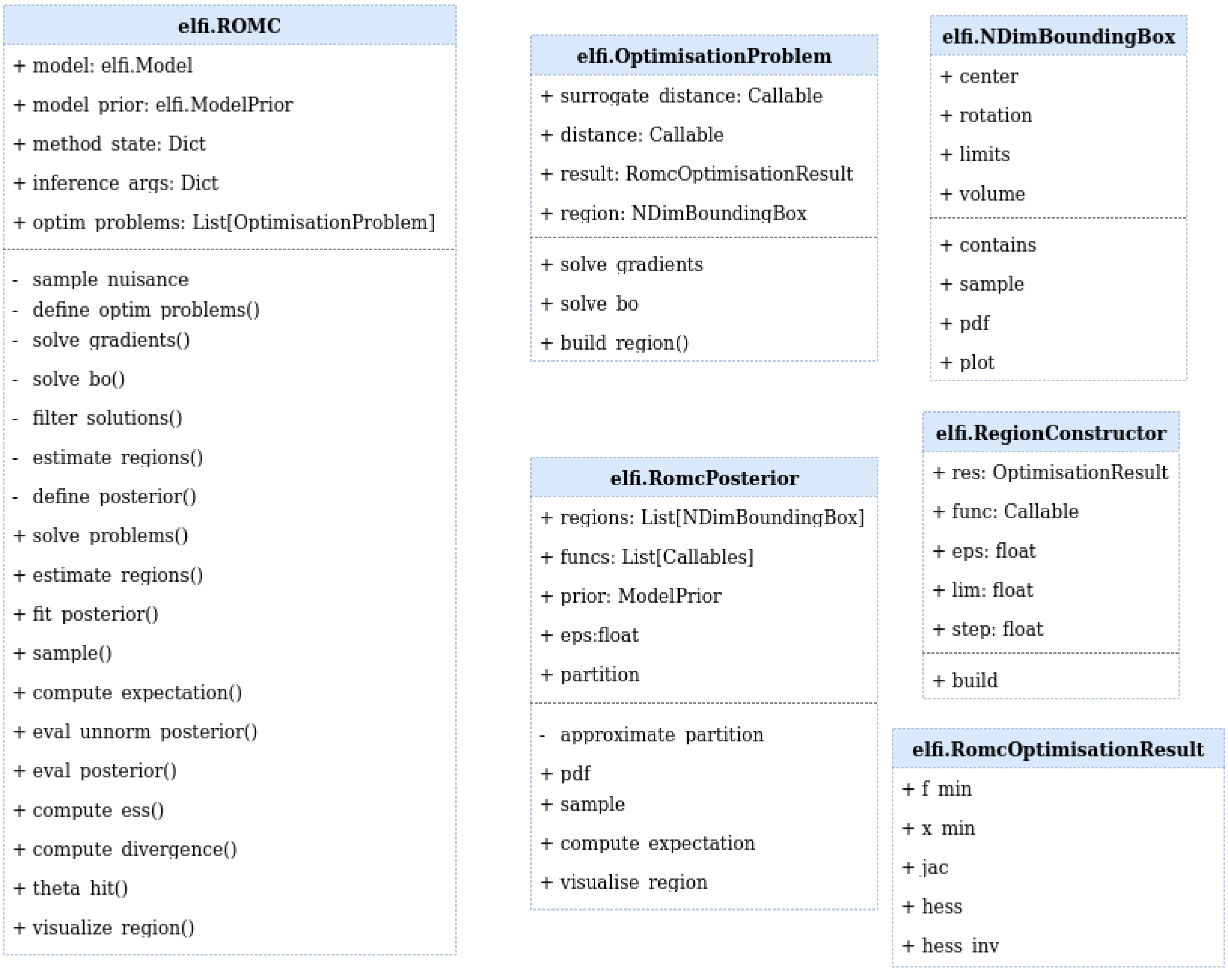

Figure 8: Histogram of distances and visualisation of a specific region.

4 Experiments

This section presents the ROMC implementation on some real-world examples. It is used to present the accuracy of the method both at a conceptual and the implementation level. The two examples that will be presented are multidimensional to confirm that method works fine in higher-dimensions. The first one is chosen to be a simple $2D$ with tractable likelihood, for the ground-truth information to be available for validation purposes. The second one is the second-degree moving average model, where the likelihood becomes intractable as the number of observations grows large. This model, which is used as a general example by the ELFI package, is chosen to illustrate that our implementation performs well at a general model, not implemented by us.

4.1 Example 1: Simple 2D example

This examples is implemented for validating that the ROMC implementation works accurately in a multidimensional parameter space.

Problem Definition

The equation that model the inference problem are presented below.

$$p(\boldsymbol{\theta}) = p(\theta_1)p(\theta_2) = \mathcal{U}(\theta_1; -2.5, 2.5)\mathcal{U}(\theta_2; -2.5, 2.5) \tag{4.1}$$

$$p(\mathbf{y}|\boldsymbol{\theta}) = \mathcal{N}(\mathbf{y}; \boldsymbol{\theta}, \mathcal{I}) \tag{4.2}$$

$$p(\boldsymbol{\theta}|\mathbf{y}) = \frac{1}{Z}p(\boldsymbol{\theta})p(\mathbf{y}|\boldsymbol{\theta}) \tag{4.3}$$

$$Z = \int_{\boldsymbol{\theta}} p(\boldsymbol{\theta})p(\mathbf{y}|\boldsymbol{\theta})d\boldsymbol{\theta} \tag{4.4}$$

Computing the unnormalised posterior is straightforward using the equation and approximating the partition Z is feasible with using the Riemann's approximation. Hence, computing the ground-truth posterior is computationally feasible. Setting the observation to $\mathbf{y_0} = (-0.5, 0.5)$, the posterior distribution is illustrated in figure 12. In table 4.1, we present the ground-truth statistics i.e. μ, σ of the marginal posterior distributions.

Performing the inference

We perform the inference using the following hyperparameters $n_1 = 500, n_2 = 30, \epsilon = 0.4$. This set-up leads to a total of 15000 samples. As observed in the histogram of distances 9, in the gradient-based approach, all optimisation problems reach an almost zero distance end point; hence all optimal points are accepted. At the Bayesian optimisation scheme, the grand majority of the optimisation procedures has the behaviour; there are only 4 optimal distance above the limit. In figure 10, the acceptance area of a specific optimisation problem is demonstrated. We observe that both optimisation schemes lead to a similar bounding box construction. This specific example is quite representative of the rest optimisation problems; due to the simplicity of the optimisation process, in most cases the optimal points are similar and the surrogate model represents accurately the local region. Hence, similar proposal regions are obtained using both optimisation alternatives.

The histograms of the marginal distributions, based on the weighted samples, is presented in figure 11. In the same figure, we can also plot the ground-truth distribution with the red dotted line. We observe that the weighted samples, follow quite accurately the ground-truth distribution. This is also confirmed by the statistics provided in table 4.1; the sample mean μ and standard deviation σ are similar to the ground-truth for both parameters θ_1 and θ_2. We also observe that they are almost the same between the two optimisation schemes.

Finally, the ground-truth and the approximate posteriors are presented in figure 12. We also confirm that the approximations are close to the ground truth posteriors. As a notice, we can observe that the approximate posteriors ... a diamond shape in the mode of the posterior; this happens due to the approximation of a circular gaussian-shape posterior with a sum of square boxes. The divergence between the ground-truth distribution and the approximate ones is 0.077, using the Jensen-Shannon distance.

In this experiment we observed that the implementation fulfilled the theoretical expectations for the ROMC inference method.

	μ_{θ_1}	σ_{θ_1}	μ_{θ_2}	σ_{θ_2}
Ground-truth	-0.45	0.935	0.45	0.935
ROMC (gradient-based)	-0.482	0.976	0.522	0.945
ROMC (Bayesian optimisation)	-0.481	0.976	0.518	0.947

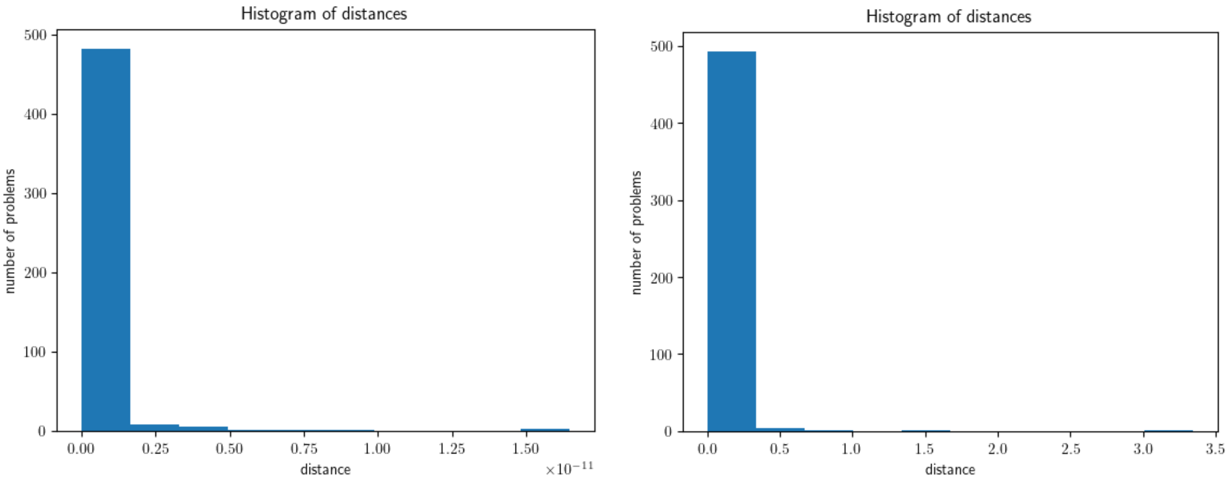

Figure 9: Histogram of distances $d^*_{i,i\in 1,\dots,n_1}$. The left graph corresponds to the gradient-based approach and the right one to the Bayesian optimisation approach.

4.2 Example 2: Second-order Moving Average MA(2)

The second examples is the The second-order moving average (MA2), which is internally implemented in the ELFI package. This example is chosen to confirm that the ROMC implementation works well under a general model, not implemented by us.

Problem definition

The second-order moving average (MA2) is a common model used for univariate time series analysis. The observation at time t is given by:

$$y_t = w_t + \theta_1 w_{t-1} + \theta_2 w_{t-2} \tag{4.5}$$

$$\theta_1, \theta_2 \in \mathbb{R}, \quad w_{k,k\in\mathbb{Z}} \sim \mathcal{N}(0,1) \tag{4.6}$$

As we can notice, $w_{k,k\in\mathbb{Z}} \sim \mathcal{N}(0,1)$ represents an independent and identically distributed white noise and θ_1, θ_2 the dependence from the previous observations. The number of consecutive observations T is a hyper-parameter of the model; in our case we will set $T = 100$. Computing the likelihood of the MA2 model is generally difficult, due to the unobserved noise variables w_t, w_{t-1}, w_{t-2}, and it becomes intractable in cases where T is large. On the other hand, generating an MA2 time-series is pretty easy and efficient using a simulator; this makes the likelihood-free inference methods quite convenient for the particular model.

At our example, we use the prior as defined by (Marin et al. 2012) for guaranteeing that the inference problem is identifiable i.e. loosely speaking, the likelihood will have just one mode. The

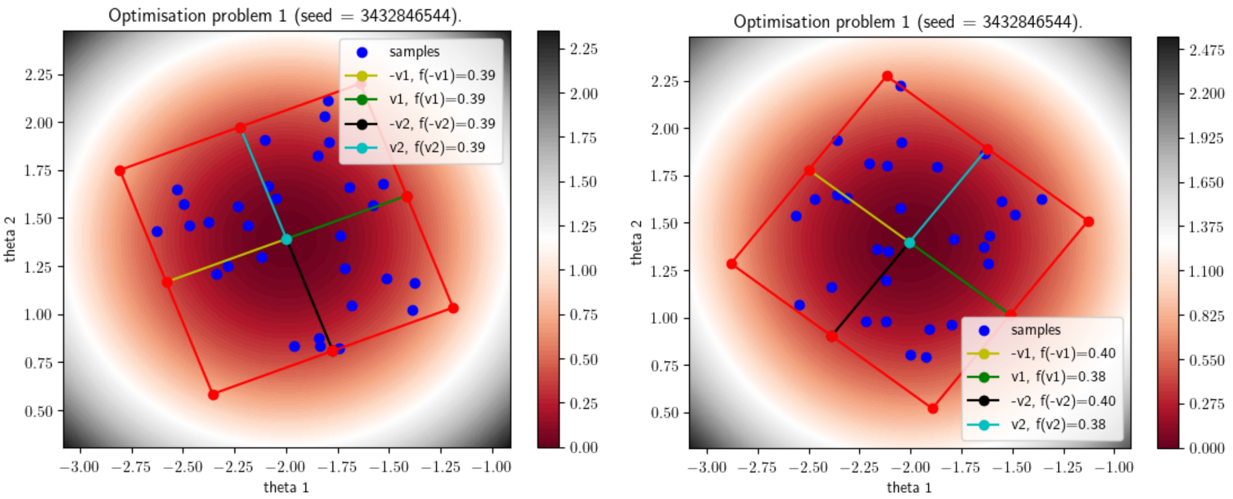

Figure 10: Visualisation of the acceptance region in 3 different optimisation problems. Each row illustrates a different optimisation problem, the left column corresponds to the gradient-based approach and the right column to the Bayesian optimisation approach. The examples have been chosen to illustrate three different cases; in the first case, both optimisation schemes lead to similar optimal point and bounding box, in the second case the bounding box is similar in shape but a little bit shifted to the right relatively to the gradient-based approach and in the third case, both the optimal point and the bounding box is completely different.

multivariate prior, which is given in the equation (4.7), follows a triangular shape as ploted in figure 13.

$$p(\boldsymbol{\theta}) = p(\theta_1)p(\theta_2|\theta_1) = \mathcal{U}(\theta_1; -2, 2)\mathcal{U}(\theta_2; \theta_1 - 1, \theta_1 + 1) \tag{4.7}$$

The vector $\mathbf{y}_0 = (y_1, \ldots, y_{100})$, used as the observation, is generated with $\boldsymbol{\theta} = (0.6, 0.2)$.

Perform the inference

As in the previous example, we perform the inference using both optimisation versions, the gradient-based and the Bayesian optimisation; in this way, we compare the results obtained in each step. Since in this example it is impossible to obtain ground-truth information, we use the samples obtained with Rejection ABC sampling for comparison.

In figure 14 we observe that in most cases the optimal distance d_i^* is close to zero in both optimisation approaches.

In figure **??**, we have chosen three different optimisation examples for illustrating three different cases. In the first case, both optimisation schemes lead to the same bounding box. In the second case, the bounding box has similar shape, different size and it is shifted along the θ_1 axis. Finally, in the third case, both the bounding box and the optimal point are completely different. This leads conclusion, that although fitting a surrogate model has important computational advantages, there is no guarantee that it will reproduce the local region around the optimal point with accuracy. This approximation error leads sometimes to the construction of quite different proposal regions, which in turn, explains the small differences in the histogram of the marginal distributions presented in figure 16 and in the approximate posteriors in figure 17.

The histograms of the marginal posteriors are similar between all approaches, as shown in figure 16. In the table 4.2 we present the empirical mean μ and standard deviation σ in all cases. We observe that there is a general agreement between the approaches, which verifies that the ROMC implementation provides sensible results. Finally, in figure 17 we provide the ROMC approximate posteriors using gradients and Bayesian optimisation; as confirmed by the statistics in 4.2, both posteriors have a single mode, located at the same point, with a larger variance observed in the Bayesian Optimisation case.

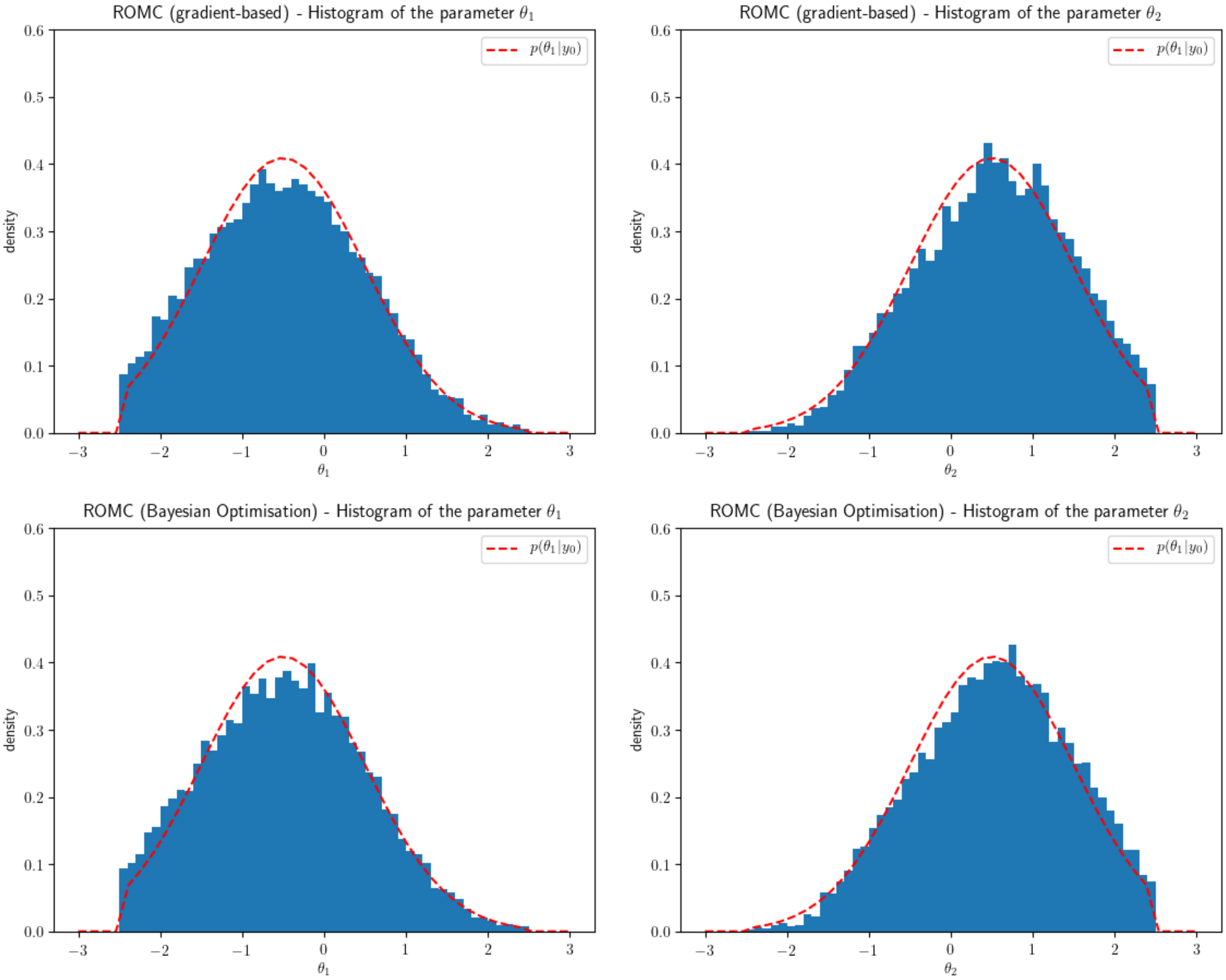

Figure 11: Histogram of the marginal distribution for three different inference approaches; (a) in the first row, the approximate posterior samples are obtained using Rejection ABC sampling (b) in the second row, using ROMC sampling with gradient-based approach and (c) in the third row, using ROMC sampling with Bayesian optimisation approach. The vertical (red) line represents the samples mean μ and the horizontal (black) the standard deviation σ.

	μ_{θ_1}	σ_{θ_1}	μ_{θ_2}	σ_{θ_2}
Rejection ABC	0.516	0.142	0.07	0.172
ROMC (gradient-based)	0.495	0.136	0.048	0.178
ROMC (Bayesian optimisation)	0.510	0.156	0.108	0.183

4.3 Execution Time Experiments

ll

5 Conclusions

5.1 Outcomes

5.2 Future Research Directions

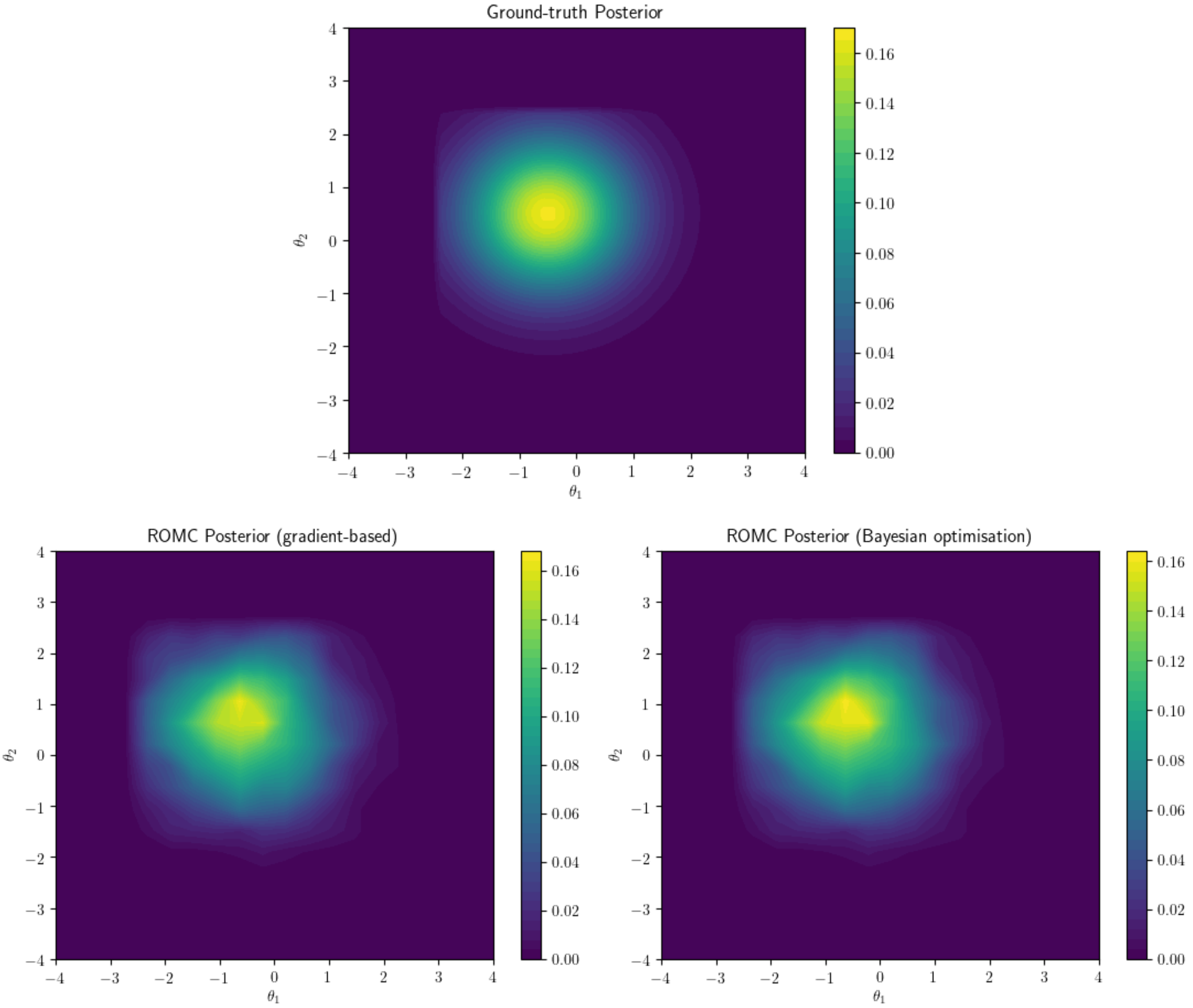

Figure 12: (a) First row: Ground-truth posterior approximated computationally. (b) ROMC approximate posteriors using gradient-based approach (left) and Bayesian optimisation approach (right).

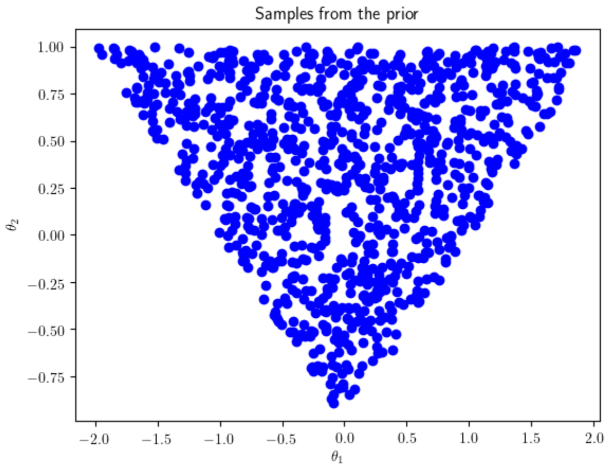

Figure 13: Prior distribution as define by Marin et al. (Marin et al. 2012).

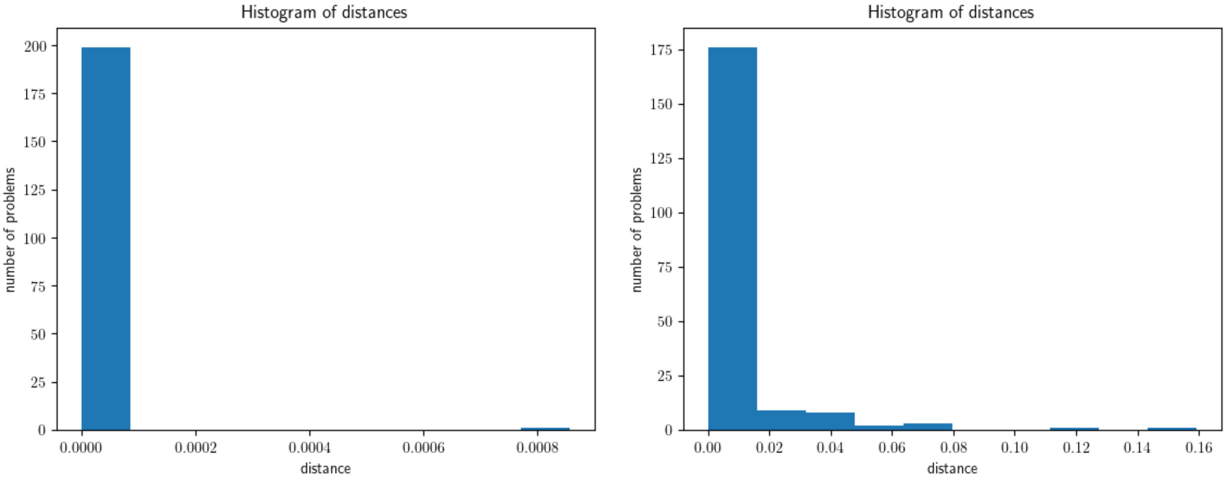

Figure 14: Histogram of distances $d^*_{i,i\in 1,\ldots,n_1}$. The left graph corresponds to the gradient-based approach and the right one to the Bayesian optimisation approach.

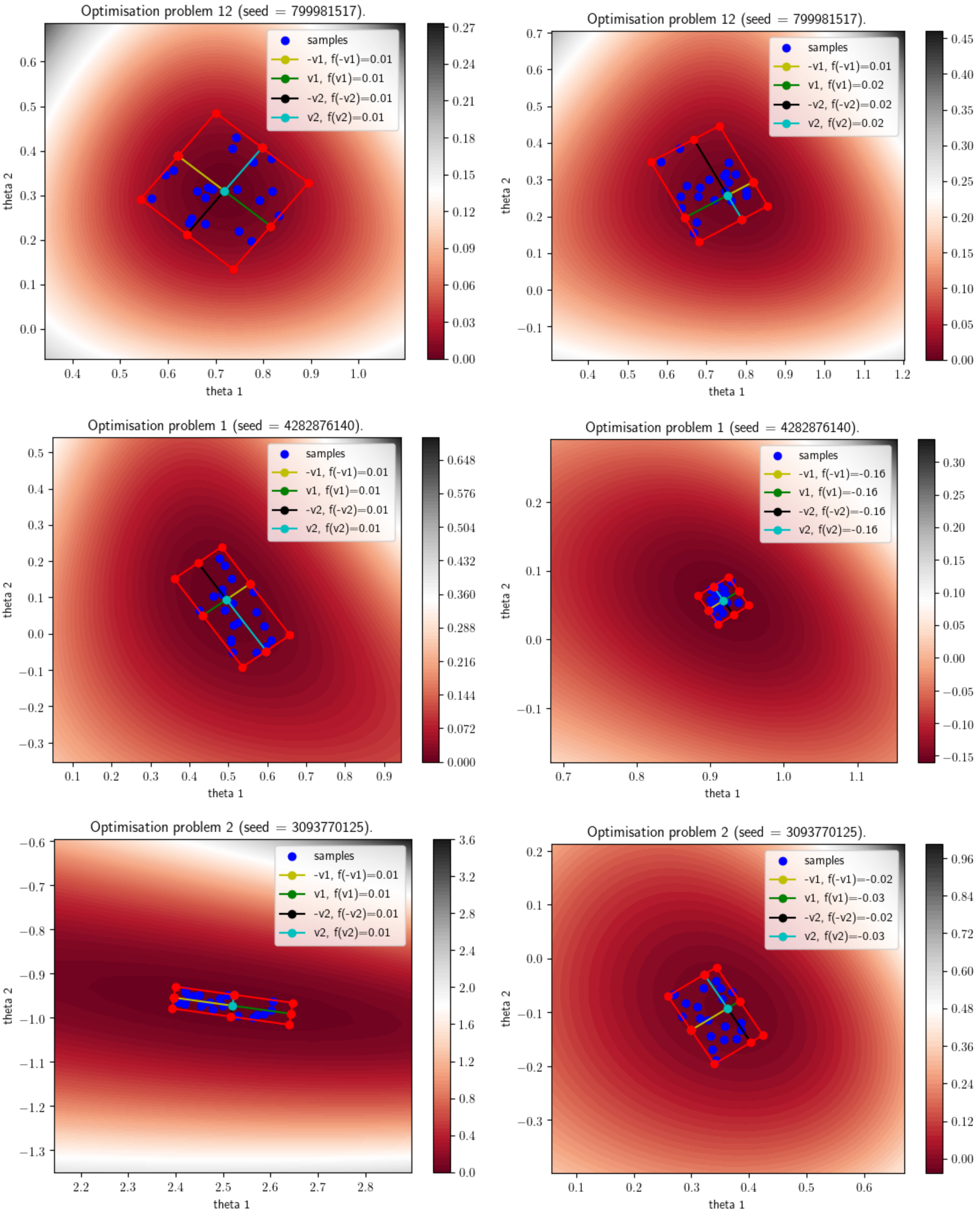

Figure 15: Visualisation of the acceptance region in 3 different optimisation problems. Each row illustrates a different optimisation problem, the left column corresponds to the gradient-based approach and the right column to the Bayesian optimisation approach. The examples have been chosen to illustrate three different cases; in the first case, both optimisation schemes lead to similar optimal point and bounding box, in the second case the bounding box is similar in shape but a little bit shifted to the right relatively to the gradient-based approach and in the third case, both the optimal point and the bounding box is completely different.

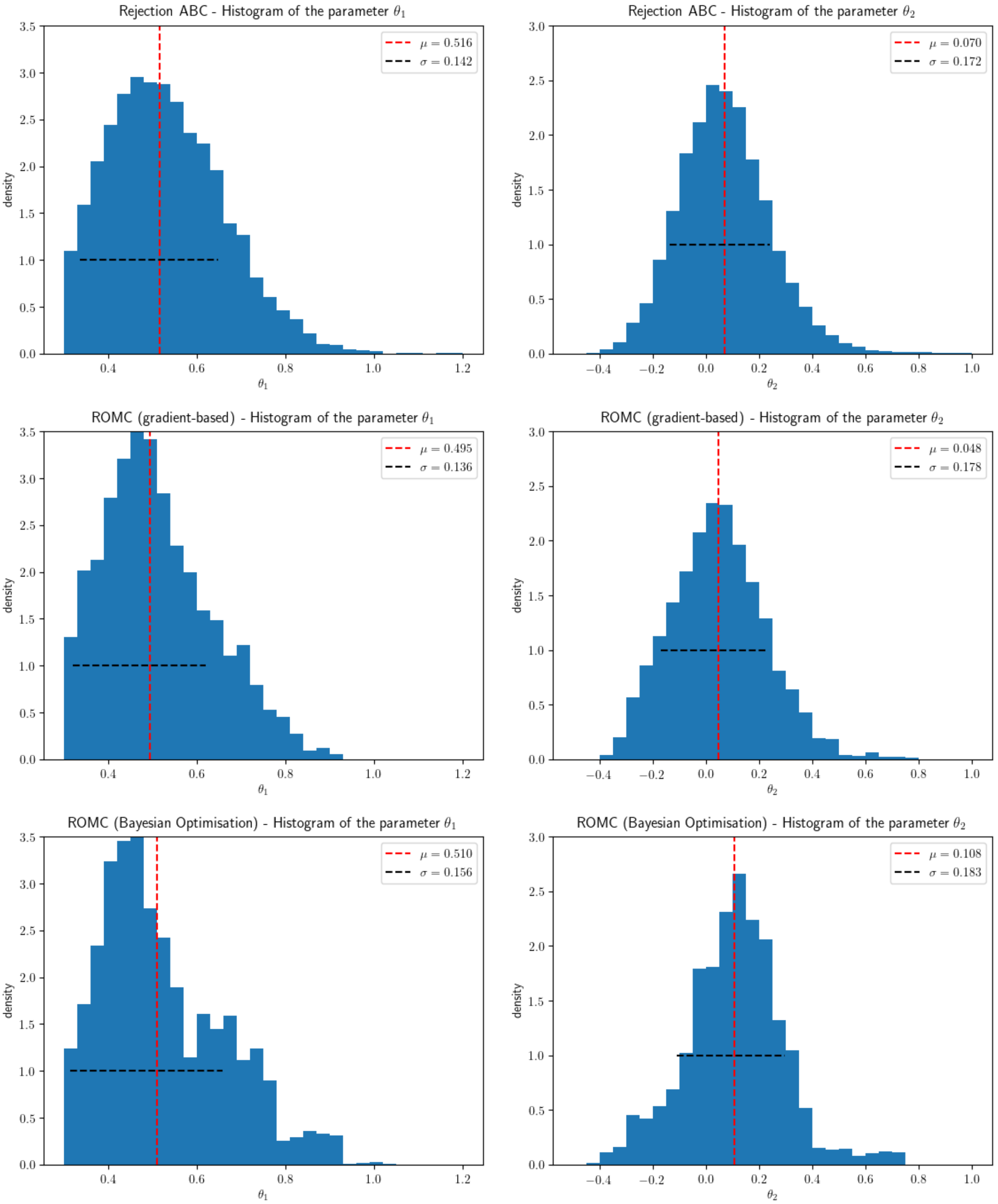

Figure 16: Histogram of the marginal distribution for three different inference approaches; (a) in the first row, the approximate posterior samples are obtained using Rejection ABC sampling (b) in the second row, using ROMC sampling with gradient-based approach and (c) in the third row, using ROMC sampling with Bayesian optimisation approach. The vertical (red) line represents the samples mean μ and the horizontal (black) the standard deviation σ.

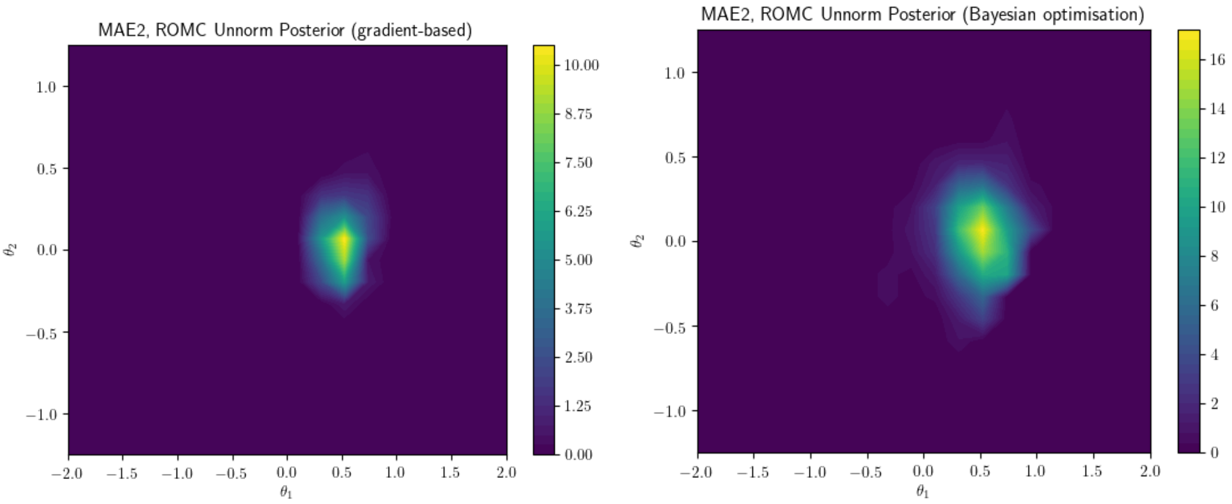

Figure 17: ROMC approximate posteriors using gradient-based approach (left) and Bayesian optimisation approach (right).

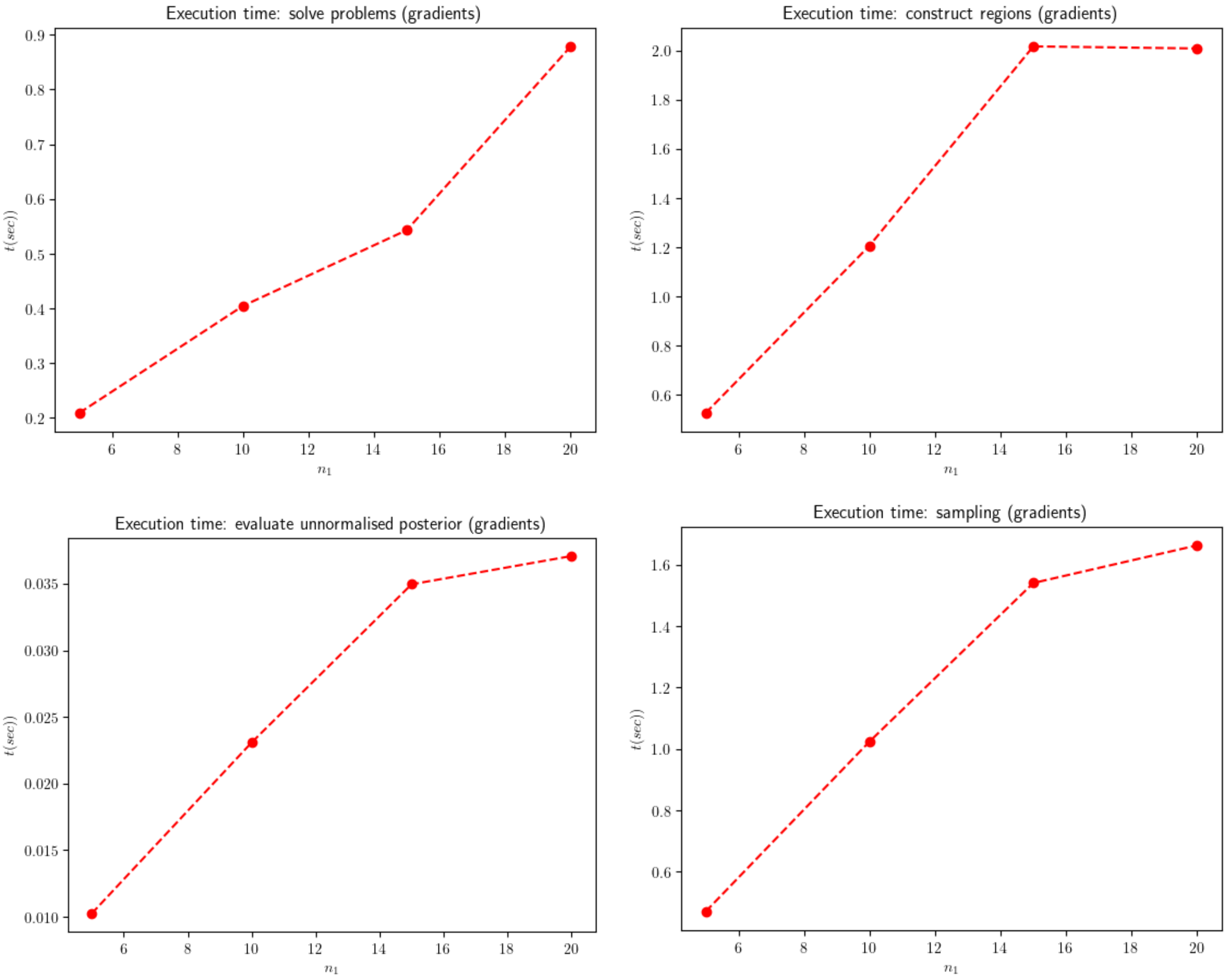

Figure 18: Gradients exec time

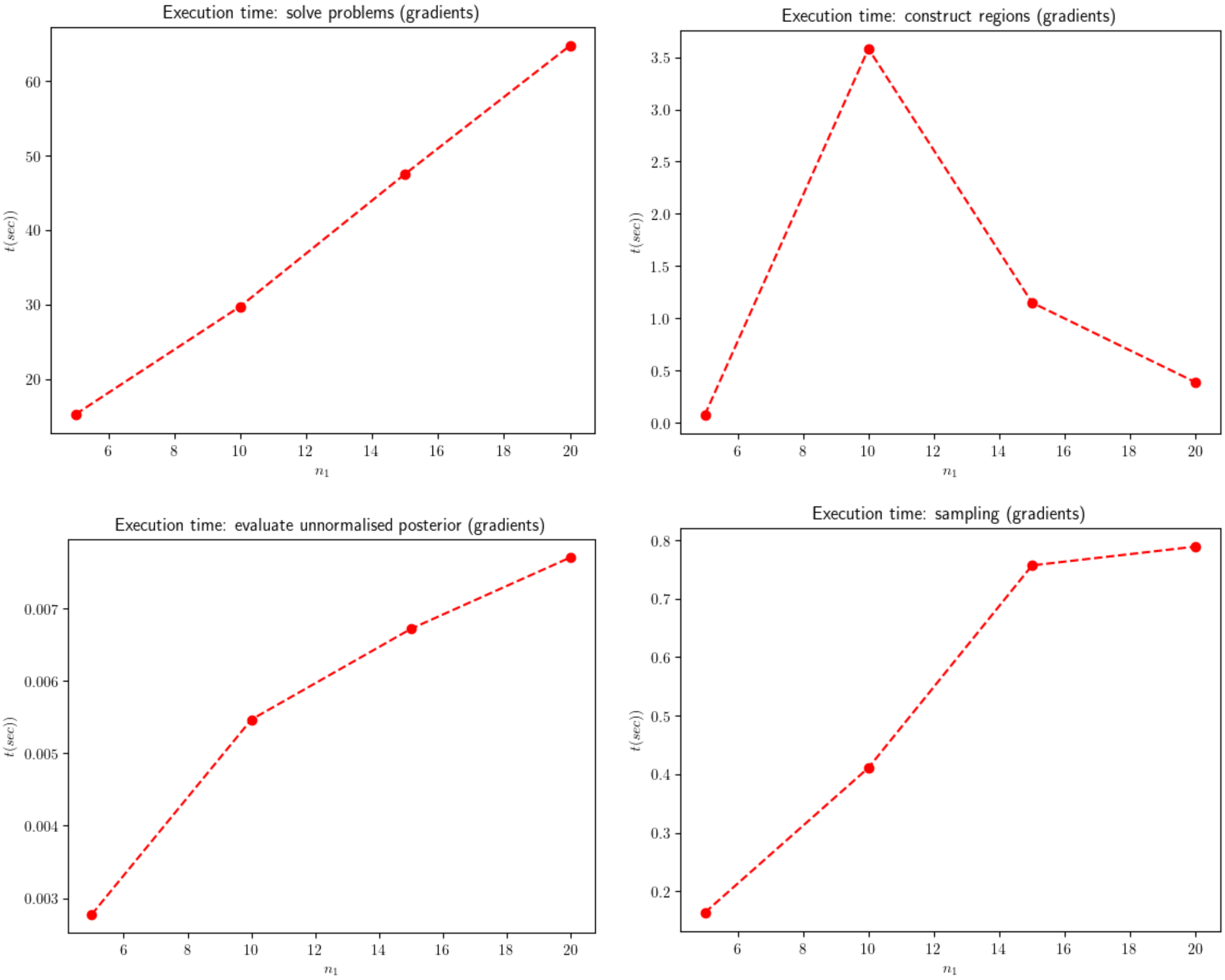
Execution time: solve problems (gradients)

Execution time: construct regions (gradients)

Execution time: evaluate unnormalised posterior (gradients)

Execution time: sampling (gradients)

Figure 19: Bo exec time

References

[CG19] Yanzhi Chen and Michael U Gutmann. “Adaptive Gaussian Copula ABC”. In: *Proceedings of Machine Learning Research*. Vol. 89. 2019, pp. 1584–1592. URL: http://proceedings.mlr.press/v89/chen19d.html.

[GC16] Michael U. Gutmann and Jukka Corander. *Bayesian optimization for likelihood-free inference of simulator-based statistical models*. 2016. arXiv: 1501.03291.

[IG19] Borislav Ikonomov and Michael U. Gutmann. “Robust Optimisation Monte Carlo”. In: (2019). arXiv: 1904.00670. URL: http://arxiv.org/abs/1904.00670.

[Lin+17] Jarno Lintusaari et al. “Fundamentals and recent developments in approximate Bayesian computation”. In: *Systematic Biology* 66.1 (2017), e66–e82. ISSN: 1076836X. DOI: 10.1093/sysbio/syw077.

[Lin+18] Jarno Lintusaari et al. *ELFI: Engine for Likelihood Free Inference*. 2018. eprint: arXiv:1708.00707.

[Mar+12] Jean Michel Marin et al. “Approximate Bayesian computational methods”. In: *Statistics and Computing* (2012). ISSN: 09603174. DOI: 10.1007/s11222-011-9288-2. arXiv: 1101.0955.

[MW15] Edward Meeds and Max Welling. “Optimization Monte Carlo: Efficient and embarrassingly parallel likelihood-free inference”. In: *Advances in Neural Information Processing Systems*. 2015. arXiv: 1506.03693.

[Sha+16] Bobak Shahriari et al. *Taking the human out of the loop: A review of Bayesian optimization*. 2016. DOI: 10.1109/JPROC.2015.2494218.

[Tan+06] Mark M. Tanaka et al. “Using approximate bayesian computation to estimate tuberculosis transmission parameters from genotype data”. In: *Genetics* (2006). ISSN: 00166731. DOI: 10.1534/genetics.106.055574.

Appendices

A An Appendix

Some stuff.

B Another Appendix

Some other stuff.